Cell Chemical Biology

CYP27A1-dependent anti-melanoma activity of limonoid natural products targets mitochondrial metabolism

Graphical abstract

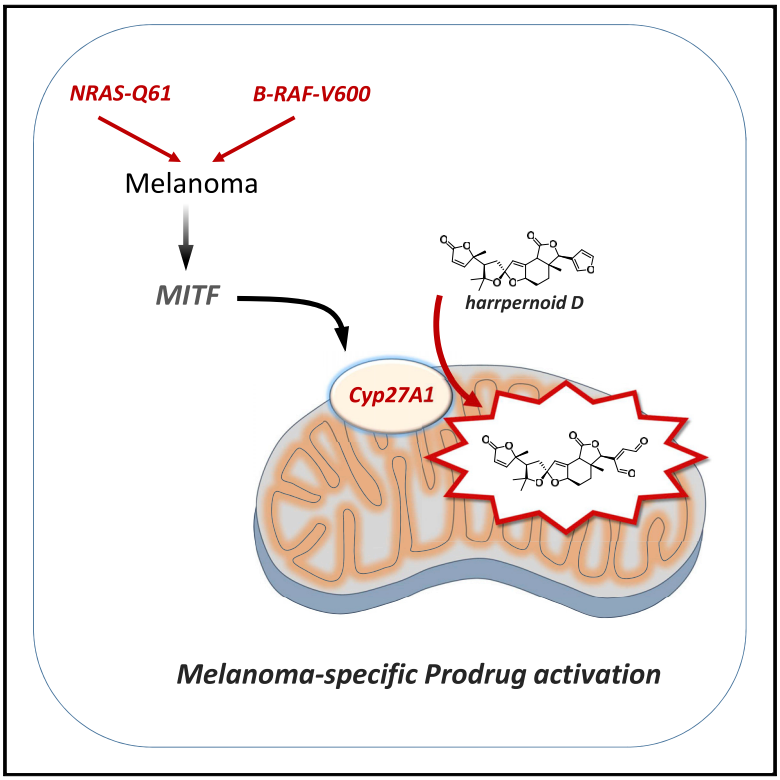

Authors

Hyelim Cho, Qiong Shen, Lydia H. Zhang, ..., Stephen M. Canham, Jeremy L. Jenkins, William C. Forrester

Correspondence

jeremy.jenkins@novartis.com (J.L.J.), william.forrester@novartis.com (W.C.F.)

In brief

Selective targeting of melanoma cells by limonoid natural products involves their conversion to a reactive electrophilic metabolite by CYP27A1, a mitochondrial cytochrome p450 enzyme, leading to toxic adducts of key mitochondrial proteins. *CYP27A1* is a target gene of MITF, the oncogenic transcription factor deregulated in melanoma.

Highlights

- The limonoid, harrpernoid D, was isolated and described
- Harrperonid D is activated by CYP27A1, to overcome BRAFi-resistant melanoma
- Metabolism of harrpernoid D into a reactive enedial modifies mitochondrial proteins

Cho et al., 2021, Cell Chemical Biology *28*, 1–13
September 16, 2021
https://doi.org/10.1016/j.chembiol.2021.03.004

CellPress

Please cite this article in press as: Cho et al., CYP27A1-dependent anti-melanoma activity of limonoid natural products targets mitochondrial metabolism, Cell Chemical Biology (2021), https://doi.org/10.1016/j.chembiol.2021.03.004

Cell Chemical Biology

CellPress

Article

CYP27A1-dependent anti-melanoma activity of limonoid natural products targets mitochondrial metabolism

Hyelim Cho,[1] Qiong Shen,[1] Lydia H. Zhang,[4,5] Mikiko Okumura,[4,5] Akinori Kawakami,[3] Jessi Ambrose,[1] Frederic Sigoillot,[1] Howard R. Miller,[1] Scott Gleim,[1] Amanda Cobos-Correa,[2] Ying Wang,[2] Philippe Piechon,[2] Guglielmo Roma,[2] Fabian Eggimann,[2] Charles Moore,[2] Peter Aspesi, Jr.,[1] Felipa A. Mapa,[1] Heather Burks,[1] Nathan T. Ross,[1] Philipp Krastel,[2] Marc Hild,[1] Thomas J. Maimone,[4,5] David E. Fisher,[3] Daniel K. Nomura,[4,5,6,7,8] John A. Tallarico,[1,5] Stephen M. Canham,[1,5] Jeremy L. Jenkins,[1,*] and William C. Forrester[1,9,*]

[1]Novartis Institutes for BioMedical Research, 181 Massachusetts Avenue, Cambridge, MA 02139, USA
[2]Novartis Institutes for BioMedical Research, Novartis Pharma AG, Forum 1 Novartis Campus, 4056 Basel, Switzerland
[3]Department of Dermatology, Massachusetts General Hospital, Harvard Medical School, Boston, MA 02114, USA
[4]Department of Chemistry, University of California, Berkeley, Berkeley, CA 94720, USA
[5]Novartis-Berkeley Center for Proteomics and Chemistry Technologies, Berkeley, CA 94720, USA
[6]Department of Molecular and Cell Biology, University of California, Berkeley, CA 94720, USA
[7]Department of Nutritional Sciences and Toxicology, University of California, Berkeley, CA 94720, USA
[8]Innovative Genomics Institute, Berkeley, CA 94720, USA
[9]Lead contact
*Correspondence: jeremy.jenkins@novartis.com (J.L.J.), william.forrester@novartis.com (W.C.F.)
https://doi.org/10.1016/j.chembiol.2021.03.004

SUMMARY

Three limonoid natural products with selective anti-proliferative activity against BRAF(V600E) and NRAS(Q61K)-mutation-dependent melanoma cell lines were identified. Differential transcriptome analysis revealed dependency of compound activity on expression of the mitochondrial cytochrome P450 oxidase *CYP27A1*, a transcriptional target of melanogenesis-associated transcription factor (MITF). We determined that CYP27A1 activity is necessary for the generation of a reactive metabolite that proceeds to inhibit cellular proliferation. A genome-wide small interfering RNA screen in combination with chemical proteomics experiments revealed gene-drug functional epistasis, suggesting that these compounds target mitochondrial biogenesis and inhibit tumor bioenergetics through a covalent mechanism. Our work suggests a strategy for melanoma-specific targeting by exploiting the expression of MITF target gene *CYP27A1* and inhibiting mitochondrial oxidative phosphorylation in BRAF mutant melanomas.

INTRODUCTION

Natural products are a rich source of bioactive compounds for drug discovery and are particularly instrumental as anticancer and antimicrobial therapeutics (Harvey, 2008; Dias, et al., 2012; Harvey, et al., 2015; Shen, 2015). A recent analysis has found that approximately 50% of approved anticancer drugs from 1940 to 2014 originated from natural products or directly derived therefrom (Newman and Cragg, 2016). Key examples are the plant-derived natural products vincristine and paclitaxel, which have been hallmark cancer therapeutics for almost 30 years (da Richa, et al., 2001). As part of an effort to identify new oncology targets and compound leads we profiled a portion of the Novartis natural product collection against a panel of 39 cell lines (lung, ovarian, colon, and brain cell lineages) to look for selective cytotoxicity profiles (Shoemaker, 2006), followed by large-scale profiling of selected compounds across cancer cell lines from diverse tissue lineages. Herein, we identified several limonoid natural products isolated from the *Harrisonia perforata* plant from Southeast Asia having a selective cytotoxicity profile. Haperforin G and haperforin C2, previously reported, and a previously uncharacterized limonoid, which we have named harrpernoid D, displayed selective anti-melanoma activity (Yan et al., 2011; Zhang et al., 2020). We identified that the melanoma-specific cytotoxicity is dependent on expression of an MITF (melanogenesis-associated transcription factor) target gene, *CYP27A1*. CYP27A1 converts haperforin G/C2 and harrpernoid D into covalently active metabolite(s) that inhibit mitochondrial biogenesis (mitobiogenesis). This tissue-specific prodrug activation enables targeting the regulation of cancer energetics as a unique opportunity to overcome resistance to BRAFi/MAPKi therapy.

RESULTS

Screening of a chemical library of 15,500 natural products

To identify selective inhibitors of cancer cell proliferation, we screened 15,500 natural products from our internal collection at 1 and 10 μM across a panel of 39 cell lines for half maximal

Please cite this article in press as: Cho et al., CYP27A1-dependent anti-melanoma activity of limonoid natural products targets mitochondrial metabolism, Cell Chemical Biology (2021), https://doi.org/10.1016/j.chembiol.2021.03.004

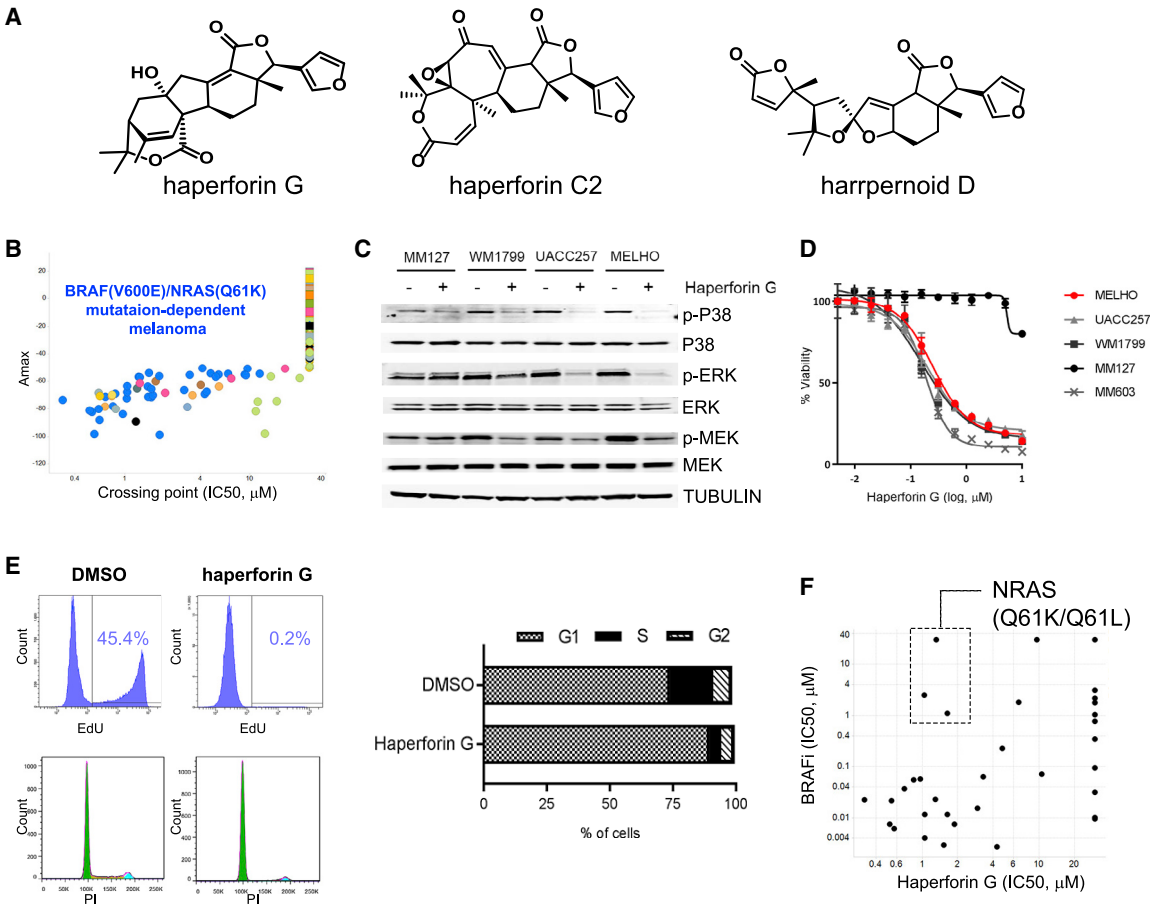

Figure 1. Identification of limonoid natural products with anti-melanoma activity

(A) Chemical structure of the limonoid natural products haperforin G, haperforin C2, and harrpernoid D.

(B) Selective cell line profile showing enrichment for BRAF(V600E)/NRAS(Q61K) mutant melanoma cell lines (blue circles) in haperforin G-sensitive cell line group. Crossing point indicates compound concentration where 50% growth inhibition by control (MG132, proteasome inhibitor) is achieved.

(C) Immunoblot analysis of phospho-MAPK pathway in cells treated with compound (0.25 μM) for 72 h. Tubulin was used for loading control.

(D) Percentage viability relative to vehicle (DMSO) control for the indicated melanoma cell lines after treatment for 96 h with the indicated doses of compound. Error bars indicate mean ± SD of three replicates.

(E) Cell proliferation assay by EdU (5-ethynyl-2′-deoxyuridine) staining (left, top) and cell cycle analysis by PI (propidium iodide) staining (left, bottom) in MELHO treated with compound (0.25 μM) for 72 h. Cell cycle analysis from treatment of haperforin G compared with DMSO control (right).

(F) Comparison of cell line profiles (skin lineage) between BRAFi and haperforin G. Indicated cell lines have mutation in NRAS (Q61K/Q61L).

inhibitory concentration (IC_{50}) determination. The ~1,400 active natural products were validated by re-testing across the 39 cell lines to generate dose-response curves (Figure S1A). From our screen, 113 natural products demonstrating reasonable potency and selectivity were prioritized for additional cytotoxicity profiling across a larger viability screen containing 498 cell lines from the Cancer Cell Line Encyclopedia (CCLE) (Data S1) (Barretina et al., 2012). From this intensive phenotypic screening we identified haperforin G (Figure 1A), which exhibits anti-proliferative activity (IC_{50} of 0.3 μM ~ 12 μM) against a broad range of melanoma cell lines harboring gain-of-function mutations in BRAF(V600E) and NRAS(Q61K) (Figure 1B; blue circles), and including cell lines with intrinsic resistance to BRAF inhibitors (BRAFi). Haperforin G downregulated MAPK pathway activation and induced proliferative arrest in sensitive cell lines (Figures 1C–1E). It also inhibited proliferation of NRAS(Q61K)-mutation-dependent melanoma cell lines which are insensitive to BRAFi (Figure 1F) suggesting that haperforin G is not a BRAF inhibitor, instead exhibiting an uncharacterized mechanism of action.

Hit expansion and structural elucidation of harrpernoid D

Our limited supply of haperforin G drove us to attempt the identification of additional small molecules structurally related to haperforin G. This expanded set was generated using five different *in silico* expansion methods: identification of bioisosteres followed by 2D similarity search (Morgan/RDKit), extended connectivity fingerprints (ECFP6) with Tanimoto and Tversky similarity, MDL public keys similarity, and Bayesian affinity fingerprints (BAFPs) (Bender et al., 2006). Our expansion to ~1,300 structurally similar compounds was tested in a synthetic lethal screen comprised of two cell lines that were sensitive (MELHO and MM603) and three cell lines that were insensitive (MM466, A375, MM127) to haperforin G treatment (Figure S1B). In our

Please cite this article in press as: Cho et al., CYP27A1-dependent anti-melanoma activity of limonoid natural products targets mitochondrial metabolism, Cell Chemical Biology (2021), https://doi.org/10.1016/j.chembiol.2021.03.004

expansion, we identified two additional compounds with similar cell proliferation selectivity profiles: haperforin C2 and a compound we have named harrpernoid D by reason of its structural similarity to harrpernoid B and C (Figures 1A and S1C) (Yan et al., 2011).

Previous reports have described the isolation and structural elucidation of highly rearranged limonoids present in the leaves of *H. perforata* (Blanco) Merr. (Simaroubaceae) collected from Southeast Asia (Yan et al., 2011; Khuong-Huu et al., 2000). Harrpernoid D, a compound isolated from *H. perforata*, has a molecular formula of $C_{25}H_{28}O_7$ as deduced from HRMS(ESI) (*m/z* 441.1908 $[M + H]^+$; found 441.1909). The NMR spectra of harrpernoid D showed the presence of a γ-lactone, furan moiety, and a ring skeleton with structural similarity to previously identified harrpernoid B and C (Yan et al., 2011) except for the presence of a double bond on ring B2, not on ring C (Figure S1C). The absolute stereochemistry and structural configuration was confirmed by X-ray crystallographic analysis. All further studies herein were performed with harrpernoid D because of our limited supply of haperforin G and C2.

Global analysis of expression-sensitivity relationships reveals correlation of haperforin G sensitivity to high *MITF* expression and CYP27A1 activity

To understand the observed selective cytotoxicity of haperforin G we compared transcriptome profiles of the identified sensitive cell lines and insensitive cell lines from all tissue lineages. Microarray and RNA-sequencing (RNA-seq) analyses revealed distinct gene signatures between sensitive and insensitive cell lines (Figures 2A and S1D). *MITF*, a skin-lineage survival oncogene amplified in malignant melanoma (Garraway et al., 2005), was highly expressed in a group of compound-sensitive cell lines from all tissue lineages. Next, we compared transcriptome profiles of compound-sensitive cell lines and insensitive cell lines with melanoma lineage. *MITF* was observed to be highly expressed in the compound-sensitive cell lines (Figure 2B). Furthermore, downstream target genes of MITF (*CYP27A1*, *TYR*, *MLANA*, *SLC45A2*, *TNFRSF14*, *LGALS3*, *PIR*, *ST6GAL6*, *ASCL1*, and *ATP6V1B2*) were also highly expressed in compound-sensitive melanoma cell lines (Du et al., 2003; Hou, et al., 2000; Hoek et al., 2008). Among those MITF target genes that showed differential expression in haperforin G-sensitive and -insensitive cell lines, *CYP27A1* expression was the most significantly correlating feature conferring compound sensitivity (Figure 2A). Gene expression analysis from the CCLE on melanoma cell lines indicated positive correlation (R^2 = 0.529) between the mRNA expression levels of *MITF* and *CYP27A1* (Figure 2C).

To validate the correlation between *CYP27A1* expression and *MITF* expression, we expressed MITF in $MITF^{low}$ melanoma cell lines. Ectopic expression of MITF increased *CYP27A1* transcription (~2.5-fold in A375 and ~5.6-fold in Lox Imvi; Figure 2D) which is consistent with reports by others (Hoek et al., 2008). Likewise, downregulation of *MITF* mRNA level by small interfering RNA (siRNA) knockdown experiments led to concomitant downregulation of *CYP27A1* mRNA levels (Figure 2E). Chromatin immunoprecipitation (ChIP) with MITF followed by qRT-PCR on the promoter region of *CYP27A1* revealed that MITF directly binds the *CYP27A1* promoter (Figure 2F). Supporting our findings, others have identified through ChIP-seq (ChIP coupled to high-throughput sequencing) with MITF the putative binding site of MITF within the promoter region of *CYP27A1* (Webster et al., 2014). Together, these findings suggest that *CYP27A1* transcription is regulated by MITF and *CYP27A1* is a transcriptional target of MITF.

Anti-melanoma activity of harrpernoid D is dependent on CYP27A1

CYP27A1 ranked as a top correlation feature between gene expression and compound sensitivity. *CYP27A1* was more highly expressed in the haperforin G-sensitive group of cell lines across all tissue lineages and there is a positive correlation between compound response value (lower IC_{50}) and *CYP27A1* expression (Figure 3A). To characterize the correlation between *CYP27A1* expression and compound sensitivity, we used two genetic approaches. First, we transiently knocked down expression of *CYP27A1* using siRNA. Transient downregulation of *CYP27A1* expression rescued cells from harrpernoid D-mediated inhibition of cell proliferation (Figure 3B). Second, we generated *CYP27A1* null cell lines using clustered regularly interspaced short palindromic repeats (CRISPR)/Cas9-mediated genome editing. Isolated single clones of biallelic *CYP27A1* knockout cells ($CYP27A1^{-/-}$) did not show loss of viability compared with wild-type cells (Figure S2A). When treated with harrpernoid D, $CYP27A1^{-/-}$ cells were rescued from compound-mediated growth inhibition and cells with monoallelic knockout of *CYP27A1* ($CYP27A1^{+/-}$) showed intermediate phenotype between $CYP27A1^{-/-}$ cells and wild-type cells. This phenotype was confirmed in three different melanoma cell lines (MELHO, UACC257, IGR37) (Figures 3C and S2B). These genetic approaches strongly suggest that *CYP27A1* is the genetic determinant that confers compound sensitivity. To further confirm that CYP27A1 activity is required for cytotoxic activity, we used combination treatment of harrpernoid D and the CYP27A1 inhibitor, fadrozole (Mast, et al., 2015). Cells co-treated with harrpernoid D and fadrozole were partially rescued from harrpernoid D-mediated growth inhibition (Figure 3D), suggesting that CYP27A1 activity is required for harrpernoid D activity.

To determine whether *CYP27A1* expression is sufficient for harrpernoid D sensitivity, we overexpressed *CYP27A1* in $CYP27A1^{low}$ cell line (MM127) and *CYP27A1* null cell line ($Cyp27A1^{-/-}$ MELHO). $CYP27A1^{-/-}$ MELHO complemented with *CYP27A1* overexpression restored harrpernoid D sensitivity and MM127 overexpressing *CYP27A1* gained sensitivity to harrpernoid D (Figure S2C), suggesting *CYP27A1* expression is sufficient for harrpernoid D sensitivity in the cell lines tested. A panel of $CYP27A1^{low}$ and $CYP27A1^{mid}$ cell lines (A375, IGR37, Lox Imvi, MEL JUSO, A101d, and WM983b) overexpressed with *CYP27A1* also became more sensitive to harrpernoid D activity (Figure S2D).

CYP27A1 biotransformation of harrpernoid D

The observed dependence of anti-melanoma activity on CYP27A1 suggested that harrpernoid D might be a prodrug converted by the cytochrome P450 oxidase, CYP27A1, into an active metabolite responsible for cytotoxicity. To determine if harrpernoid D was converted into an active metabolite, we expressed human CYP27A1 in *Bacillus megaterium* and incubated

Please cite this article in press as: Cho et al., CYP27A1-dependent anti-melanoma activity of limonoid natural products targets mitochondrial metabolism, Cell Chemical Biology (2021), https://doi.org/10.1016/j.chembiol.2021.03.004

A

Gene	Wilcox P-value(nominal)	Effect size
CYP27A1	1.29E-08	6.1
GEMIN2	2.58E-08	-0.76
GPR137B	9.03E-08	2.5
LINC00673	9.03E-08	2.3
BAMBI	1.55E-07	3.8
MITF	2.45E-07	4.7
SH3TC2	2.45E-07	1.8
GPNMB	3.87E-07	7.6
KANK1	3.87E-07	2.0

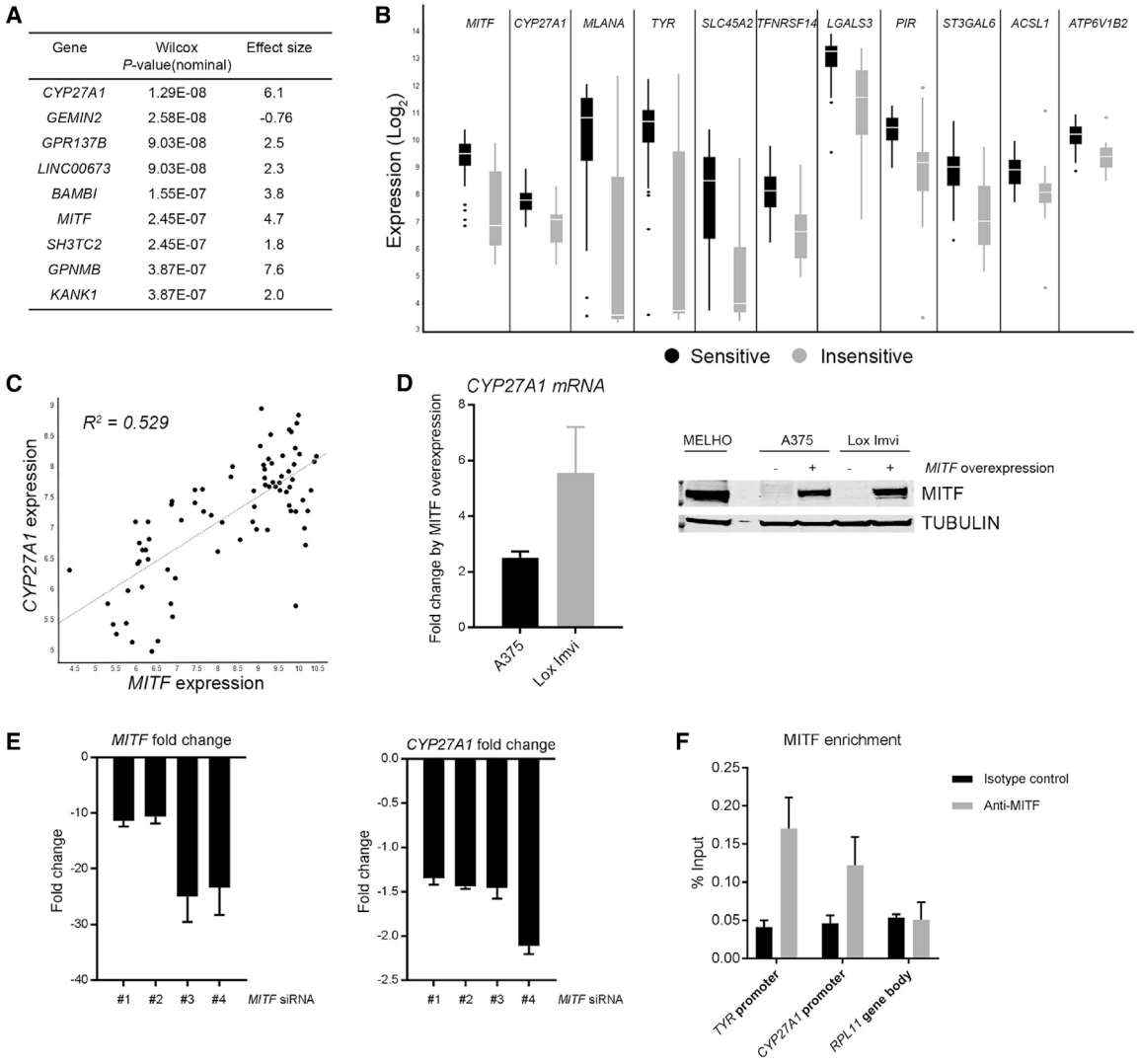

Figure 2. Global analysis of expression-sensitivity relationships reveals correlation of compound sensitivity to high *MITF* expression

(A) Genes showed differential expression in sensitive and insensitive cell lines identified by transcriptome profiling. Cells from all tissue lineages were included in the analysis. Effect size was determined by calculating mean difference between sensitive and insensitive lines divided by standard deviation.

(B) MITF^{high} cell lines are more sensitive to haperforin G. Expression levels of *MITF* and its transcriptional target genes were compared between haperforin G-sensitive (36 cell lines) and -insensitive cell lines (19 cell lines) from skin lineage (cell lines used in Data S4).

(C) Correlation between the mRNA expression levels of *MITF* and *CYP27A1* in cell lines from skin lineage. The coefficient of determination (R^2) is indicated.

(D) Cells were infected with either empty lentiviral vector or lentiviral vector expressing MITF. CYP27A1 mRNA level was measured by qRT-PCR.

(E) Cells (*MITF*^{high}) were transfected with siRNA targeting *MITF* and *CYP27A1* mRNA level was measured by qRT-PCR.

(F) Binding of MITF to the endogenous *CYP27A1* promoter region in melanoma cell line (UACC257). The data show relative promoter occupancy. *TYR* is established MITF target and was used as a positive control. *RPL11* gene body was used as a negative control.

with harrpernoid D (Ehrhardt, et al., 2016). Testing cholestenone in the *B. megaterium* system expressing CYP27A1 gave clear conversion to a number of hydroxylated products (Figure S3A). When harrpernoid D was incubated with wild-type *B. megaterium*, no conversion or degradation was observed over a 48-h time period (Figure S3B). However, when harrpernoid D was incubated with *B. megaterium* expressing human CYP27A1 there was an observed ~30% loss of the parent compound after 8 h and complete disappearance after 24 h (Figure S3C). Unexpectedly, no identifiable metabolites of harrpernoid D were isolated despite several extraction attempts (Figure S3D). We presumed the furan ring of harrpernoid D is activated by CYP27A1 to generate a reactive enedial. Related natural products teucrin A, 8-epidiosbulbin E acetate, and diosbulbin B similarly convert into reactive enedials, which covalently modifies cysteine and lysine residues (Druckovia and Marnett, 2006; Lin et al., 2016; Lin et al., 2014; Druckova, et al., 2007; Kornienko and La Clair, 2017).

As a chemically controlled mimetic of P450 oxidation, harrpernoid D was treated with dimethyldioxirane (DMDO), which induced oxidation and ring opening of the furan to a chemically sensitive enedial that was observed by ^{1}H NMR spectroscopy

Please cite this article in press as: Cho et al., CYP27A1-dependent anti-melanoma activity of limonoid natural products targets mitochondrial metabolism, Cell Chemical Biology (2021), https://doi.org/10.1016/j.chembiol.2021.03.004

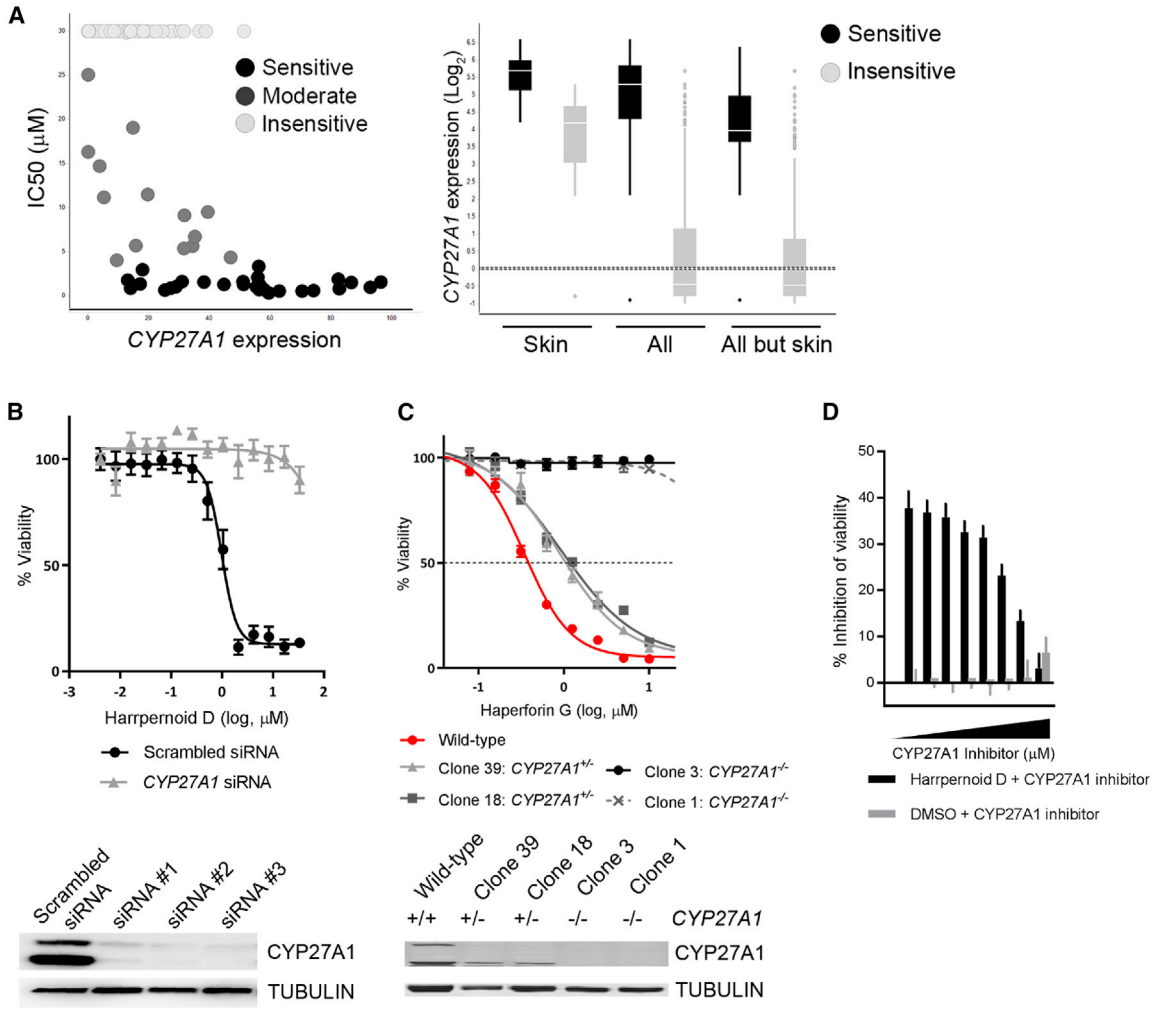

Figure 3. Global analysis of expression-sensitivity relationships showing harrpernoid D activity is CYP27A1-dependent

(A) (Left) Correlation of *CYP27A1* expression (RNA-seq) and compound sensitivity. Each dot indicates individual cell line from all tissue lineages. (Right) Differential expression of *CYP27A1* in compound-sensitive and -insensitive cell lines. Skin, skin lineage; All, all tissue lineage; All but skin, all tissue lineage except for skin lineage.

(B) Percentage viability (relative to DMSO-treated cells) of MELHO treated with indicated concentrations of compound for 96 h. Cells were transfected with either scrambled siRNA or siRNA against *CYP27A1* 24 h prior to compound treatment.

(C) Percentage viability of wild-type MELHO was compared with monoallelic knockout clones ($CYP27A1^{+/-}$) and biallelic knockout clones ($CYP27A1^{-/-}$) after compound treatment.

(D) Cells were treated with 2.5 μM harrpernoid D (or DMSO) in combination with increasing dose of CYP27A1 inhibitor, fadrozole. Data are shown as percentage inhibition of viability.

and high-resolution mass spectrometry (Figures 4A and S3E). Treatment of this electrophilic species with *N*-acetyl cysteine methyl ester generated a complex mixture of labile products in analogy to prior observations with teucrin A (Druckovia and Marnett, 2006). Thus, if such a reactive enedial of harrpernoid D is generated biologically by CYP27A1, rapid formation of protein adducts may have obscured our ability to directly detect any metabolites from the *B. megaterium* biotransformation experiments.

ABPP to map harrpernoid D targets in melanoma cells

To capture the putative targets that might be covalently modified by the active metabolite of harrpernoid D, we applied an isotopic tandem orthogonal proteolysis-enabled activity-based protein profiling (isoTOP-ABPP) approach pioneered by Cravatt and Weerapana (Weerapana et al., 2010) and subsequently adapted for use in the context of a competitive assay (Wang, et al., 2014; Backus et al., 2016). When used in a competitive manner, covalent small molecules can compete against binding of a broadly reactive probe to facilitate the discovery of proteins and ligandable sites targeted by the covalently acting compound. In this study we treated either wild-type and $CYP27A1^{-/-}$ HCT116 cells with vehicle or 50 μM harrpernoid D followed by competitive labeling of proteomes with cysteine-reactive alkyne-functionalized iodoacetamide probe (IA-alkyne) (Figure S4A). Isotopically light or heavy cleavable enrichment handles were appended to probe-labeled proteins for isoTOP-ABPP analysis. Enriched

Please cite this article in press as: Cho et al., CYP27A1-dependent anti-melanoma activity of limonoid natural products targets mitochondrial metabolism, Cell Chemical Biology (2021), https://doi.org/10.1016/j.chembiol.2021.03.004

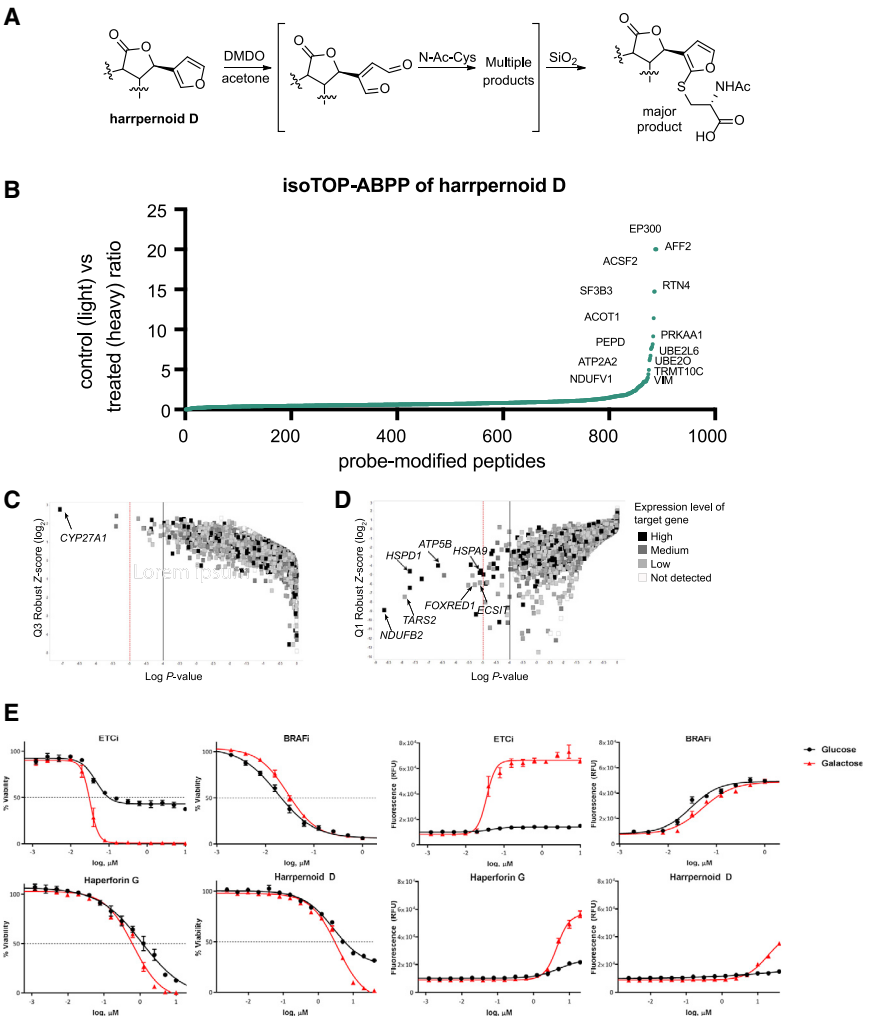

Figure 4. Genome-wide siRNA-compound epistasis screening reveals mitochondrial pathway-specific mechanism of action of harrpernoid D

(A) Chemical oxidation of harrpernoid D with DMDO generates a reactive α,β-unsaturated enedial electrophile.

(B) isoTOP-ABPP of harrpernoid D (50 μM) in wild-type, *CYP27A1*^{high} HCT116 cells.

(C and D) Scatterplot of Q3 or Q1 of Robust *Z* score versus RSA for eight individual siRNAs per gene. Each dot represents an individual target gene in the siRNA library, shaded according to expression level (RNA-seq) in the cell line used (MELHO). Cutoff lines indicate selected thresholds of p value 10E-5 (red) and 10E-4 (black). Marked genes are selected hits, which increased resistance to compound (C) or increased sensitivity to compound (D).

(E) Sensitivity to antimycin A (ETCi), dabrafenib (BRAFi), haperforin G, and harrpernoid D was determined in UACC257 cells cultured in growth media containing glucose or galactose to promote glycolysis or mitochondrial OxPhos, respectively. Viability (left four panels) determined with CellTiter-Glo and membrane integrity was determined using CellTox Green (right four panels) 96 h after addition of compounds.

probe-modified tryptic peptides were analyzed by liquid chromatography-tandem mass spectrometry (LC-MS/MS) and heavy to light tryptic probe-modified peptide ratios, representing control versus treated IA-alkyne-labeled sites, were quantified. Harrpernoid D-treated wild-type, *CYP27A1*^{high} HCT116 cells had an enrichment in a number of mitochondrial and ER proteins compared with the comparably treated *CYP27A1*$^{-/-}$ HCT116 cells (Figure 4B and Data S2). Interestingly, teucrin A and furan, which are activated by CYP3A, have been shown to covalently target mitochondrial proteins and enzymes responsible for lipid, amino acid, and drug metabolism (Druckova, et al., 2007; Moro et al., 2012; Lekehal et al., 1996).

Genome-wide siRNA-compound epistasis screening reveals mitochondrial pathway-specific mechanism of action for harrpernoid D

In an effort to add clarity to the chemoproteomics data, we performed a genome-wide siRNA-compound epistasis screen. Three independent viability screens were conducted in the presence of harrpernoid D, BRAF inhibitor (dabrafenib), or control (DMSO) to identify the genes that alter the cellular viability in response to harrpernoid D but not to BRAFi or control treatment. Both redundant siRNA activity (RSA) and GESS (genome-wide enrichment of seed sequences) off-target analysis identified *CYP27A1* as a hit (target gene of depleted siRNA) that suppresses sensitivity to harrpernoid D (but not to BRAFi) (Figures 4C and S3B, and Data S3). In addition, GESS analysis revealed that knockdown of ferredoxin 1 (FDX1), which assists in transferring electrons from NADPH to CYP27A1 (Pikuleva, et al., 1999), also suppressed compound activity (Figure S3C). Notably, knocking down genes that are involved with oxidative phosphorylation (OxPhos)/mitochondrial electron transport chain (ETC) complex sensitized cells to harrpernoid D (but not to BRAFi). Those genes include mitochondrial chaperones (*HSPA9* and *HSPD1*), a mitochondrial tRNA synthetase (TARS2), a mitochondrial protein transporter (*TIMM23*), and ETC complex subunit/assembly factors (*NDUFB2*, *ATP5B*, *FOXRED1*, and *ECSIT*) (Figure 4D). Based on the epistasis between harrpernoid D and silencing mitochondrial pathway genes, we hypothesized that regulating mitochondrial pathway components is functionally relevant for the mechanism of action for harrpernoid D. To validate a mitochondrial pathway-specific mechanism of action, we used a cell-based assay where cells were grown under conditions that shift the metabolic balance toward OxPhos (Lai et al., 2013). Cells that are metabolically adapted for growth under hypoxic and anaerobic conditions under high-glucose media can derive most of their energy from glycolysis rather than mitochondrial OxPhos. When galactose is substituted for glucose as source of energy, however, cells rely nearly exclusively on OxPhos for ATP synthesis and are more sensitive to compounds that block mitochondrial function

Please cite this article in press as: Cho et al., CYP27A1-dependent anti-melanoma activity of limonoid natural products targets mitochondrial metabolism, Cell Chemical Biology (2021), https://doi.org/10.1016/j.chembiol.2021.03.004

than cells grown in media with glucose (Marroquin et al., 2007). We observed a mild increased sensitivity to haperforin G, harrpernoid D, and strong sensitivity to an established mitochondrial ETC inhibitor (ETCi) antimycin A, but not to BRAFi (dabrafenib), of cells cultured in galactose-containing media compared with those cultured in glucose-containing media (Figure 4E). These observations together with the pathway epistasis from the siRNA screen suggest that harrpernoid D impairs mitochondrial function as a primary effect rather than secondary to other cytotoxic mechanisms. RNA-seq analysis of cell lines treated with harrpernoid D corroborated these observations. Functional gene set enrichment analysis (GSEA) revealed that a significant fraction of genes associated with mitochondrial homeostasis and mitochondrial stress response pathway is downregulated at an early time point (48 h after treatment) and upregulated at a later time point (72 h after treatment) in cells treated with harrpernoid D ($-\text{Log}_{10}\,P < 5$; Figure S5). This finding indicates that harrpernoid D affects mitochondrial homeostasis and leads to mitochondrial stress response pathway activation at the later time point (72 h after treatment). We did not find any evidence of regulation of mitochondrial pathway genes after harrpernoid D treatment in *CYP27A1*$^{-/-}$ cells (Figure S5).

Harrpernoid D inhibits mitochondrial biogenesis and maintenance of mitochondrial integrity

To evaluate harrpernoid D-induced effects on mitochondrial biogenesis, we compared the expression level of two proteins (SDH-A and MT-COX1), which are each subunits of a different OxPhos enzyme complex. Complex IV includes several proteins that are encoded in the mitochondrial genome, while the proteins of complex II are entirely encoded in the nucleus. MT-COX1 is the subunit I of complex IV (COX-I) encoded by mitochondrial DNA (mtDNA), and SDH-A is a subunit of complex II encoded by nuclear DNA (nDNA). The expression level of MT-COX1 is markedly decreased by harrpernoid D treatment in two cell lines that are sensitive to harrpernoid D (MELHO and UACC257) but not in an insensitive cell line (MM127) (Figure 5A), while the expression level of SDH-A was not changed by harrpernoid D treatment. Of note, the apparent molecular weight of SDH-A from harrpernoid D-treated cells was slightly larger compared with control cells, which might be due to the mitochondrial signal peptides that are not efficiently processed. This was also observed in other subunits of OxPhos complex (ATP5A of complex V, UQCRC2 of complex III, and SDH-B of complex II) (Figure S6A).

RNA-seq analysis showed that downregulation of MT-COX1 expression occurs at the transcriptional level. MtDNA encodes 13 mRNAs (*MT-ND1*, *MT-ND2*, *MT-ND3*, *MT-ND4*, *MT-ND4L*, *MT-ND5*, *MT-ND6*, *MT-CYB*, *MT-CO1*, *MT-CO2*, *MT-CO3*, *MT-ATP*, and *MT-ATP8*), each of which encodes a polypeptide component of the mitochondrial OxPhos system (Anderson et al., 1981; Mishra and Chan, 2014; Chinnery and Hudson, 2013). Notably, the levels of all 13 mRNAs expression were downregulated over the course of harrpernoid D treatment, which was consistent with progressive proliferative arrest (Figures 5B and S6B). We next assessed the effects of harrpernoid D on mitochondria abundance using two types of mitochondria-specific dyes (MitoTracker Green, which stains total mitochondria, and MitoTracker Red, which stains respiring mitochondria). Harrpernoid D treatment reduced the total level of mitochondria (Figure S6C). To provide an independent confirmation of the decrease in the number of mitochondria in cells treated with harrpernoid D, we quantified the amount of mtDNA present in the cells in relation to genomic DNA by quantitative PCR (Wen, et al., 2013). While harrpernoid D treatment in *CYP27A1*$^{-/-}$ cells did not alter the relative mtDNA copy number, it significantly reduced the mtDNA copy number in wild-type cells (Figure S6D). To rule out the possibility of direct inhibitory effect on mitochondrial membrane potential by harrpernoid D, we measured mitochondrial membrane potential at two different time points. Harrpernoid D did not decrease mitochondrial membrane potential at early time point (2 h after treatment), whereas an established uncoupler CCCP (2-[2-(3-chlorophenyl)hydrazinylyidene]propanedinitrile) significantly reduced membrane potential, suggesting that harrpernoid D does not directly inhibit mitochondrial membrane potential as a primary effect (Figure S6E). The modest reduction of membrane potential at the later time point (24 h after treatment) is likely due to a secondary inhibitory effect of harrpernoid D on the mitochondrial pathway.

Because the transcription of all 13 mRNAs was downregulated, we hypothesized that the transcriptional regulator of mtDNA, TFAM (transcriptional factor A, mitochondrial) might be associated with the inhibitory action of harrpernoid D on mitochondrial biogenesis. To interrogate this possibility, we performed high-content imaging analysis to visualize co-localization of TFAM with mitochondria. In control cells, TFAM is co-localized to the mitochondria, which are composed of a reticulum of distinct tubular and round mitochondria. However, cells treated with harrpernoid D display more dispersed localization of TFAM throughout the cell periphery (Figure 5C). To further analyze the localization of TFAM upon harrpernoid D treatment, we performed subcellular fractionation in harrpernoid D-sensitive (MELHO and UACC257) and -insensitive cell lines (MELHO *CYP27A1*$^{-/-}$). While the level of TFAM in whole-cell lysates remained relatively constant after harrpernoid D treatment, the level of TFAM in the mitochondrial fraction was markedly decreased in harrpernoid D-sensitive cell lines (Figure 5D). Reduction of TFAM localization to mitochondria was also observed by treatment with MKT-077 a HSPA9 inhibitor (Figure S6F). HSPA9 serves as a key regulatory component for the import of mitochondrial proteins (Schneider et al., 1994), and inhibition of HSPA9 by MKT-077 perturbed the mitochondrial import of reporter protein, MTS-EGFP (mitochondrial targeting sequence of COX8 fused to EGFP). However, harrpernoid D did not disrupt the mitochondrial import of MTS-EGFP, suggesting harrpernoid D may not directly inhibit mitochondrial protein targeting (Figure S6G). Taken together, these results effectively demonstrate inhibition of mitochondrial biogenesis by harrpernoid D.

Targeting mitobiogenesis by harrpernoid D can overcome drug resistance to BRAFi/MAPKi

Several studies have reported that inhibition of BRAF by small molecules induces an OxPhos gene program and increases mitochondrial biogenesis. Especially, treatment of BRAF-mutated melanomas with BRAFi renders them addicted to OxPhos and such adaptive metabolic program limits the efficacy

Please cite this article in press as: Cho et al., CYP27A1-dependent anti-melanoma activity of limonoid natural products targets mitochondrial metabolism, Cell Chemical Biology (2021), https://doi.org/10.1016/j.chembiol.2021.03.004

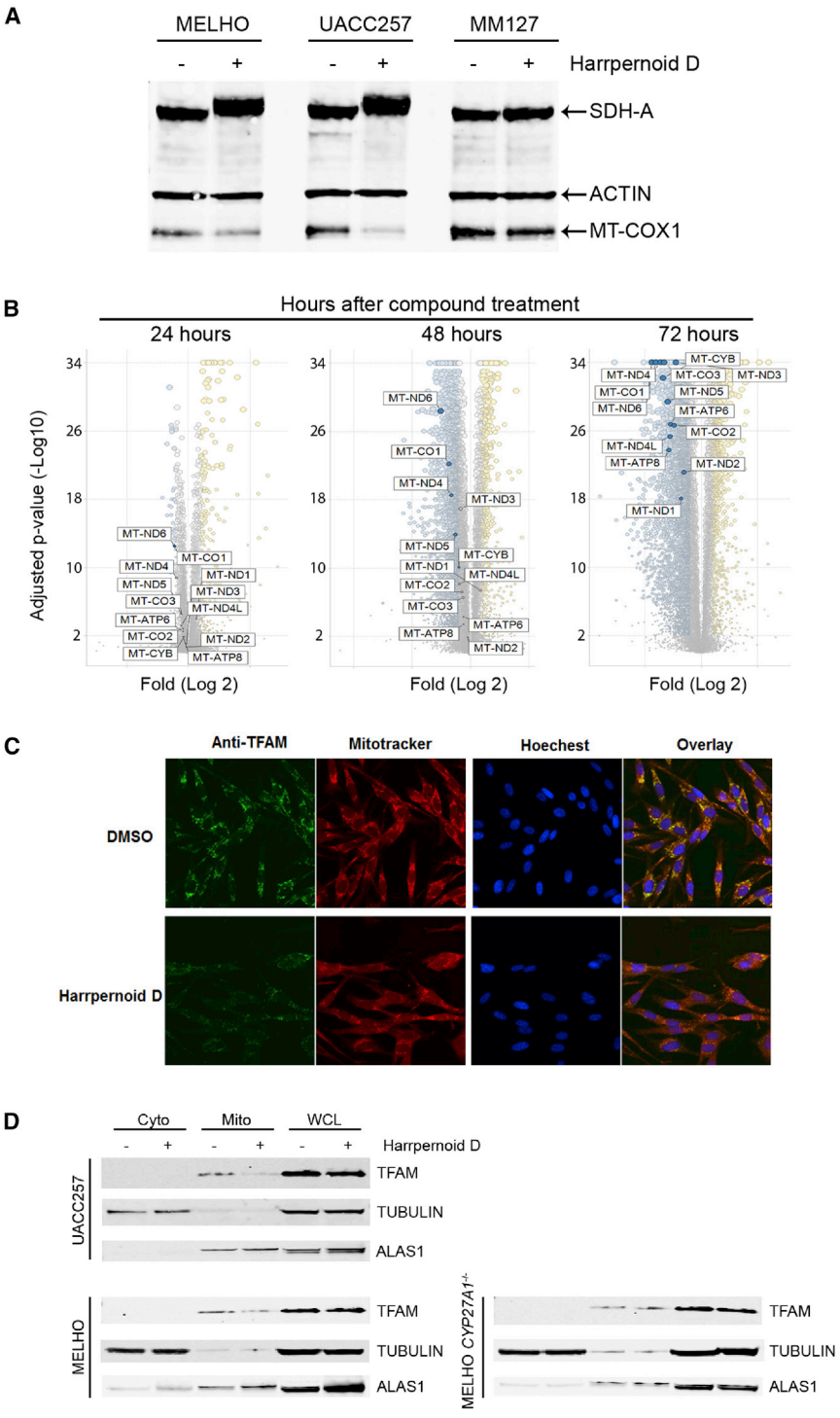

Figure 5. Harrpernoid D inhibits mitochondrial biogenesis

(A) Immunoblot analysis of mitobiogenesis-associated protein (SDH-A and MT-COX1) in cells treated with harrpernoid D 2.5 μM (IC_{50}) for 72 h. ACTIN was used as a loading control.

(B) Volcano plot of genes from RNA-seq analysis on cells treated with 4.1 μM compound (IC_{70}) for indicated time. X axis, log_2 fold change relative to DMSO control at each time point. Genes encoded by mtDNA are marked.

(C) Representative high-content images of cells treated with compound (IC_{50}) for 72 h and stained with an antibody for TFAM (green), mitochondria (red), and nucleus (blue).

(D) Subcellular fractionation and immunoblot analysis on TFAM in indicated cell lines treated with compound (IC_{50}) or DMSO control. TUBULIN, cytoplasmic loading control; ALAS1, mitochondrial loading control. Data are representative of at least three independent experiments. Amount of protein loaded: 5 μg (Cyto, cytoplasmic fraction), 5μg (Mito, mitochondrial fraction), and 25 μg (WCL, whole-cell lysate).

of BRAFi (Haq et al., 2013; Baenke et al., 2016; Corazao-Rozas et al., 2013; Canor and Sabatini, 2012).

To assess the opportunity to target mitobiogenesis and overcome resistance to BRAF/MAPK inhibition by harrpernoid D, we generated melanoma cell lines (MELHO and UACC257) that have acquired resistance to BRAFi (dabrafenib) or combination of BRAFi (dabrafenib) and MEKi (trametinib) (Figure S6H). Consistent with a previous report (Baenke et al., 2016), cells with acquired resistance displayed increased level of maximal respiratory capacity compared with the parental cells (Figure S6I). To assess the efficacy of harrpernoid D in limiting proliferation of cells with acquired resistance to BRAFi, we treated the cells with a combination of BRAFi (dabrafenib) and harrpernoid D or haperforin G. Combination of BRAFi and harrpernoid D treatment resulted in synergistic anti-proliferative activity as determined by the Bliss independence model (Keith, et al., 2005). Notably, combination of harrpernoid D and BRAFi effectively inhibited proliferation of cells with acquired resistance to BRAFi (Figure 6A). Similar results were obtained with a triple combination of harrpernoid D, BRAFi, and MEKi. Harrpernoid D and haperforin G could drive profound anti-proliferative response in cells that have acquired resistance to combination of BRAFi and MEKi (Figure 6B). Collectively, these data support that harrpernoid D can enhance the therapeutic benefits of BRAF/MAPK inhibition, and combined treatment of harrpernoid D and BRAFi/MAPKi may overcome acquired resistance to BRAFi/MAPKi.

DISCUSSION

Here we report the anti-melanoma activity and mechanism of action of three limonoid natural products. Limonoids are highly

Please cite this article in press as: Cho et al., CYP27A1-dependent anti-melanoma activity of limonoid natural products targets mitochondrial metabolism, Cell Chemical Biology (2021), https://doi.org/10.1016/j.chembiol.2021.03.004

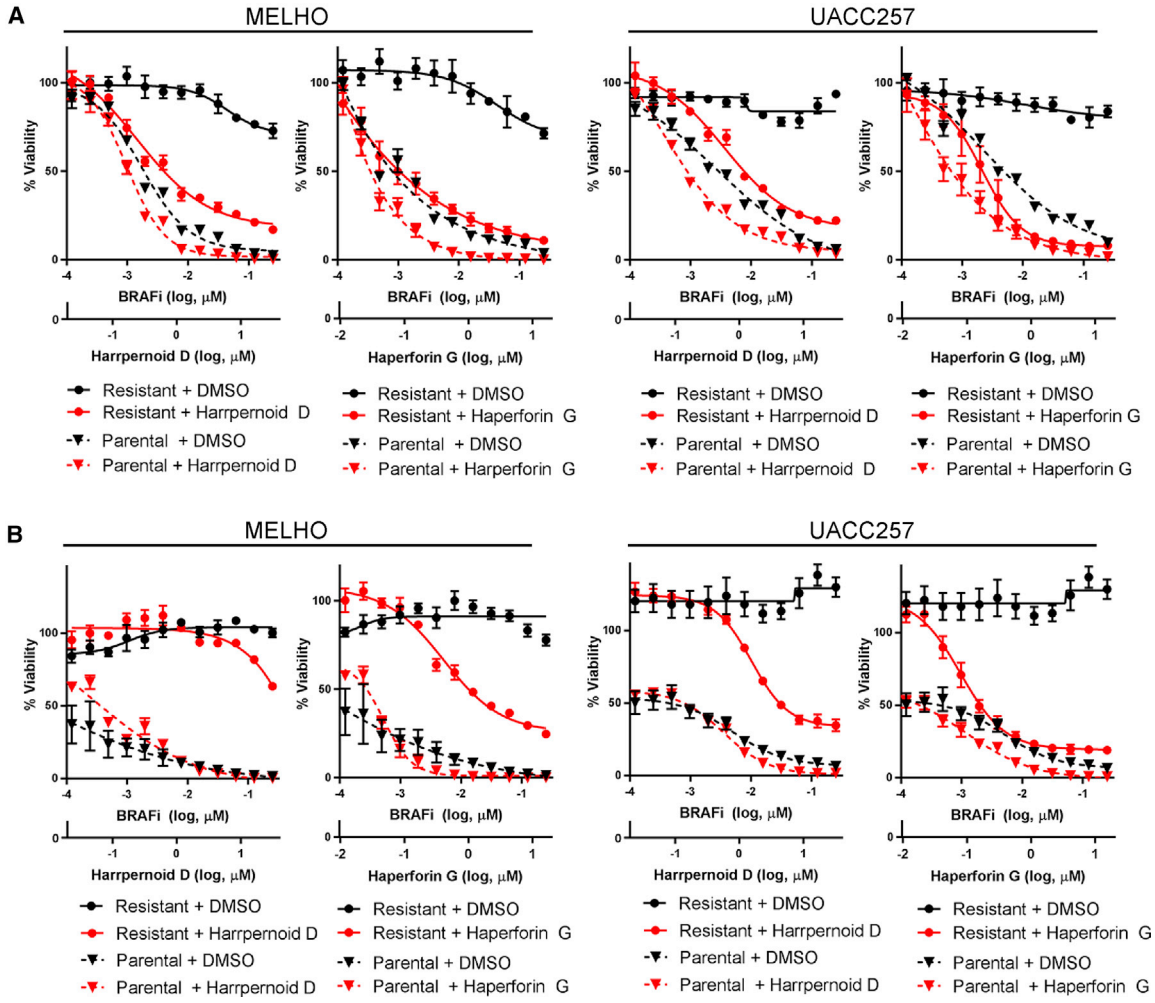

Figure 6. Combinatory treatment of harrpernoid D with BRAFi/MAPKi can overcome acquired resistance to BRAFi/MAPKi

Percentage viability relative to vehicle (DMSO) control for the indicated melanoma cell lines (parental cells) and cells with acquired resistance to BRAFi(A) or combination of BRAFi and MEKi (B) after treatment for 120 h with indicated concentrations of compound.

(A) Cells were treated with the indicated concentrations of BRAFi in combination with harrpernoid D.

(B) Cells were treated with indicated concentrations of BRAFi with fixed dose (IC_{50}) of MEKi in combination with harrpernoid D. Error bars indicate mean ± SD of at least three replicates.

oxygenated nortriterpenoids found in the Meliaceae, Rutaceae, Cneoraceae, and the *Harrisonia* of Simaroubaceae (Yan et al., 2011). Limonoids exhibit a large structural diversity and a range of biological activities such as insecticidal, antibacterial, antimalarial, antiviral, and anticancer (MacKinnon et al., 1997; Roy and Saraf, 2006; Manners, 2007; Yan et al., 2016). A large-scale cell line profiling on 498 cell lines across 25 tissue lineages allowed us to identify unique anti-melanoma activity of limonoid natural products isolated from *H. perforata*. Global transcriptome analysis on unique gene signatures of sensitive versus insensitive cells revealed that *MITF*^{high} melanoma cells are enriched for sensitivity. MITF is considered a lineage survival or lineage addiction oncogene required for both tissue-specific cancer development and tumor progression (Garraway et al., 2005; Shtivelman et al., 2014) and hence is an important target to limit proliferation of melanoma. Of note, ChIP-seq identified the putative binding site of MITF within the promoter region of *CYP27A1* (Webster et al., 2014) and modulation of *MITF* expression resulted in concomitant regulation of *CYP27A1* expression, consistent with a previous report (Hoek et al., 2008), suggesting that *CYP27A1* is a transcriptional target of MITF. Our data with genetic manipulation of *CYP27A1* and chemical perturbation of CYP27A1 activity established that harrpernoid D activity is dependent on *CYP27A1* expression and its enzyme activity, which contributes to the enrichment of MITF^{high} cells among group of cells that are sensitive to harrpernoid D. This is the first case of an anti-melanoma compound, to our knowledge, where a transcriptional target gene of MITF is required for anti-proliferative activity of a compound. At least 15% of human melanomas have *MITF* gene amplification (Garraway et al., 2005; Hodis et al., 2012) and this correlates with poor prognosis of malignant melanoma. This might indicate innovative opportunities for melanoma-specific targeting by compound(s) that are highly dependent on

Please cite this article in press as: Cho et al., CYP27A1-dependent anti-melanoma activity of limonoid natural products targets mitochondrial metabolism, Cell Chemical Biology (2021), https://doi.org/10.1016/j.chembiol.2021.03.004

expression of MITF or transcriptional target gene(s) of MITF, such as *CYP27A1*.

CYP27A1 is a mitochondrial cytochrome P450 enzyme that can hydroxylate vitamin D3 and cholesterol at carbons 25 and 26, respectively (Tieu et al., 2012; Gupta, et al., 2007). Because of the structural similarity of haperforin G, haperforin C2, and harrpernoid D to vitamin D3 and cholesterol, it seemed possible that CYP27A1 metabolized the parent precursors to a biologically active form. Similar prodrug activation of furanoid natural products such as teucrin A are activated by CYP3A enzymes to their active enedial, which can covalently modify cysteine and lysine residues of proteins (Druckova, et al., 2007). Biotransformation, synthetic manipulation, as well as isoTOP-ABPP experiments confirmed the conversion of harrpernoid D to an active enedial metabolite that covalently modifies cysteine residues of mitochondrial and ER proteins. It will be of future interest to investigate the mechanism of toxicity at the level of metabolite-target specificity. For example, whether a combination of targets identified by chemoproteomic approaches acts in concert and if there are other modifier proteins that contribute to the observed cytotoxic effects.

To investigate proteins that direct anti-melanoma activity we ran a genome-wide siRNA-compound epistasis screen that confirmed mitobiogenesis as a target pathway of harrpernoid D. It is unknown at this time why liver cancer cell lines in our CCLE profiling showed little sensitivity to haperforin G compared with melanoma lines, given the high expression of CYP27A1 in normal liver for its cholesterol metabolism function (Figure S1E). We speculate that other cytochrome p450 metabolic enzymes in liver cell lineages process the limonoids to an inactive form, ameliorating toxicity by the CYP27A1-induced metabolite. This proposal is supported by the fast clearance of harrpernoid D by human and rat liver microsomes [human, half-life ($t_{1/2}$) 3.9 min, intrinsic clearance (CL_{int}) 356 μL/min/mg protein; rat, $t_{1/2}$ < 1.98 min, CL_{int} > 700 μL/min/mg protein].

Targeting mitobiogenesis might be effective in improving the efficacy of BRAFi/MAPKi and preventing the acquisition of drug resistance to BRAFi/MAPKi (Zhang et al., 2016; Baenke et al., 2016). A previous study on human melanoma xenograft models showed that tumors with acquired resistance to vemurafenib showed continued dependency on BRAF(V600E)/MAPK signaling owing to elevated *BRAF*(V600E) expression (Das Thakur et al., 2013). Increased *BRAF*(V600E) expression is in part due to *BRAF* copy number amplification as shown in pre-clinical and clinical cases of melanoma (Shi et al., 2012; Wagle et al., 2014), and one of the most significant regions of copy gain was located on chromosome 7q34, which contains both *BRAF* and *NDUFB2* (Lin et al., 2008; Miller et al., 2010). *NDUFB2* encodes a polypeptide that is a subunit of the NADH:ubiquinone oxidoreductase (complex I of ETC complex) catalyzing the first step of mitochondrial OxPhos. Therefore, increased level of mitochondrial respiration in melanoma with acquired resistance to BRAFi as shown previously by others (Baenke et al., 2016; Corazao-Rozas et al., 2013) and by our study might be attributed to collateral co-amplification of a neighboring OxPhos gene with BRAF.

Approximately 60% of malignant melanomas harbor the $BRAF^{V600}$ missense mutation, resulting in constitutively activated MAPK signaling (Davies et al., 2002). BRAF inhibitors, such as dabrafenib and vemurafenib, elicit rapid antitumor responses; however, intrinsic and acquired resistance and clonal evolution of melanoma during BRAFi/MAPKi therapy often lead to a rapid tumor relapse by reactivation of MAPK or PI3K pathway and limits the overall response and therapeutic benefit of BRAFi/MAPKi therapy (Shi et al., 2014). Metabolic reprogramming is a hallmark of cancer modulated in part through deregulating cellular energetics to support effective neoplastic proliferation (Hanahan and Weinberg, 2011). The Warburg effect illustrates that aerobic glycolysis is the predominant metabolic pathway for cancer cells to support continuous cell growth and proliferation (Warburg, 1956). However, slow-cycling melanoma cells that are characterized by high expression levels of the histone demethylase JARID1B predominantly utilize mitochondrial OxPhos to generate ATP and are intrinsically resistant to multiple drugs such as cisplatin and vemurafenib (Roesch et al., 2013). BRAF-mutated melanoma cells treated with vemurafenib caused upregulation of the MITF/PGC1A signaling axis, resulting in metabolic reprogramming toward OxPhos and conferring intrinsic resistance to BRAF inhibitors (Haq et al., 2013). A subset of tumor biopsies from patients with disease progression despite BRAFi/MAPKi treatment showed increased mtDNA content and upregulated mitochondrial biogenesis and tumor bioenergetics (Zhang et al., 2016). Efforts have been made to address the clinical and biological relevance of targeting mitochondrial biogenesis (mitobiogenesis) and tumor bioenergetics in the context of intrinsic and acquired drug resistance (Zhang et al., 2016; Baenke et al., 2016; Schockel et al., 2015; Corazao-Rozas et al., 2013).

We therefore suggest that inhibition of mitobiogenesis might indicate emerging opportunities for combination therapies with BRAFi/MAPKi to maximize patient benefit and to deploy rational design of therapeutic combination for durable disease control. Our study characterizes harrpernoid D as a CYP27A1-activated prodrug that regulates proliferation and survival of melanoma cells by targeting mitobiogenesis.

SIGNIFICANCE

Melanoma cells are able to overcome BRAF inhibitors, such as vemurafenib, by upregulating OxPhos, inducing resistance. Combination therapy targeting OxPhos dependency with BRAF inhibition has previously been demonstrated. In this study, we identified a set of compounds that disrupt mitochondrial biogenesis in melanoma-lineage-specific cells. Melanoma lines sensitive to compound treatment had high expression of MITF, a melanocytic transcriptional master regulator. Expression of *CYP27A1*, a transcriptional target of MITF, was essential for cytotoxic activity of these compounds. These compounds, members of the limonoid natural product family, were determined to be prodrugs activated by CYP27A1 to generate a broadly reactive enedial metabolite. This transient enedial metabolite covalently modify ER and mitochondrial proteins and disrupts mitochondrial biogenesis. These finding suggest the possibility of exploiting tissue-selective inhibition of mitochondrial biogenesis through a lineage-specific prodrug mechanism. Such an approach could expand the therapeutic window for the suppression of OxPhos dependency in BRAF mutant melanomas.

STAR★METHODS

Detailed methods are provided in the online version of this paper and include the following:

- KEY RESOURCES TABLE
- RESOURCE AVAILABILITY
  - Lead contact
  - Materials availability
  - Data and code availability
- EXPERIMENTAL MODEL AND SUBJECT DETAILS
- METHOD DETAILS
  - Cell line profiling
  - Cell lines and Cell culture
  - Cell line manipulation
  - Generation of BRAFi/MAPKi resistant cell lines
  - Cell viability/cytotoxicity assay
  - Glucose-Galactose assay
  - Cell cycle analysis/cell proliferation assay
  - ChIP-qPCR
  - Western blot analysis
  - Subcellular fractionation
  - High-content imaging
  - mtDNA copy number analysis
  - Quantitation of mitochondrial membrane potential
  - Metabolic assays
  - Genome-wide RNAi screening
  - RNA-sequencing (RNA-seq)
  - Isolation of harrpernoid D
  - Chemical oxidation of harrpernoid D
  - CYP27A1 biotransformation assay
  - IsoTOP-ABPP
  - Mass spectrometry analysis
- QUANTIFICATION AND STATISTICAL ANALYSIS

SUPPLEMENTAL INFORMATION

Supplemental information can be found online at https://doi.org/10.1016/j.chembiol.2021.03.004.

ACKNOWLEDGMENTS

D.E.F. gratefully acknowledges grant support from NIH (5P01 CA163222-07 and 5R01 AR043369-24) and the Dr. Mirian and Sheldon G. Advanced Medical Research Foundation. We thank the teams of the NIBR postdoctoral program, CBT High Throughput Biology, CBT Data Science, GDC Natural Product Unit, and CBT Genomics Sciences (Novartis, Cambridge, MA, and Basel, Switzerland) and Shu Li (Analytical Sciences, Novartis, Cambridge, MA) for collaboration and support. We thank Yi Yang for pU6g-cas9-puromycin (Novartis, Cambridge, MA). We appreciate crystallography support from Ina Dix and Trixie Wagner (Novartis, Basel, Switzerland). We thank Markus Schirle and Jason R. Thomas for helpful discussion. We also thank the members of the David Fisher laboratory (Massachusetts General Hospital, Boston, MA) and Stephen Helliwell (Novartis, Basel, Switzerland) for critical reading of the manuscript and discussions.

AUTHOR CONTRIBUTIONS

H.C. designed and led the study under the supervision of W.F., J.J., and M.H. H.C. and Q.S. performed all of molecular and cellular experiments. A.K. performed ChIP experiments with MITF under the supervision of D.E.F. L.H.Z. and D.K.N. designed and ran the isoTOP-ABPP experiments. T.J.M. and M.O. designed and ran chemical oxidation experiments. F.E., C.M., and P.K. designed and ran the biotransformation experiments. H.C. and J.A. designed and performed siRNA screening under the supervision of N.R. J.L.J. performed *in silico* expansion of compound. H.C., P.A., J.A., and H.T.M. performed cellular screening of compound under the supervision of N.T.R. and F.A.M. F.S. analyzed siRNA data. G.R. and S.G. performed RNA-seq and analysis. A.C. performed natural products screening. Y.W. contributed to compound isolation, purification, and characterization. P.P. performed X-ray crystallographic analysis. S.M.C., P.K., N.R., J.A.T., D.E.F., M.H., D.K.N., T.J.M., J.L.J., and W.C.F. contributed to the study design. S.M.C., H.C., J.L.J., and W.C.F. wrote the manuscript with input from all authors.

DECLARATION OF INTERESTS

All authors (except otherwise noted) are or were at the time of their involvement with the research employees of Novartis Institutes for BioMedical Research and may hold stock in Novartis. This study was funded by the Novartis Institutes for BioMedical Research and the Novartis-Berkeley Center for Proteomics and Chemistry Technologies. D.K.N. is a co-founder, shareholder, and adviser for Frontier Medicines. D.E.F. has a financial interest in Soltego, a company developing salt-inducible kinase inhibitors for topical skin-darkening treatments that might be used for a broad set of human applications. The interests of D.E.F. were reviewed and are managed by Massachusetts General Hospital and Partners HealthCare in accordance with their conflict of interest policies.

Received: October 25, 2020
Revised: January 24, 2021
Accepted: March 9, 2021
Published: March 31, 2021

REFERENCES

Anderson, S., Bankier, A.T., Barrell, B.G., de Bruijn, M.H.L., Coulson, A.R., Drouin, J., Eperon, I.C., Nierlich, D.P., Roe, B.A., Sanger, F., et al. (1981). Sequence and organization of the human mitochondrial genome. Nature *290*, 457–465.

Backus, K.M., Correia, B.E., Lum, K.M., Forli, S., Horning, B.D., Gonzalez-Paez, G.E., Chatterjee, S., Lanning, B.R., Teijaro, J.R., Olson, A.J., et al. (2016). Proteome-wide covalent ligand discovery in native biological systems. Nature *534*, 570–574.

Baenke, F., Chaneton, B., Smith, M., Van Den Broek, N., Hogan, K., Tang, H., Viros, A., Martin, M., Galbraith, L., Girotti, M.R., et al. (2016). Resistance to BRAF inhibitors induces glutamine dependency in melanoma cells. Mol. Oncol. *10*, 73–84.

Barretina, J., Caponigro, G., Stransky, N., Venkatesan, K., Margolin, A.A., Kim, S., Wilson, C.J., Lehar, J., Kryukov, G.V., Sonkin, D., et al. (2012). The cancer cell line encyclopedia enables predictive modelling of anticancer drug sensitivity. Nature *483*, 603–607.

Bender, A., Jenkins, J.L., Glick, M., Deng, Z., Nettles, J.H., and Davies, J.W. (2006). Bayes affinity fingerprints" improve retrieval rates in virtual screening and define orthogonal bioactivity space: when are multitarget drugs a feasible concept? J. Chem. Inf. Model. *46*, 2445–2456.

Birmingham, A., Selfors, L.M., Forster, T., Wrobel, D., Kennedy, C.J., Shanks, E., Santoyo-Lopez, J., Dunican, D.J., Long, A., Kelleher, D., et al. (2009). Statistical methods for analysis of high-throughput RNA interference screens. Nat. Methods *6*, 569–575.

Canor, J., and Sabatini, D. (2012). Cancer cell metabolism: one hallmark, many faces. Cancer Discov. *2*, 881–898.

Carson, C., Raman, P., Tullai, J., Xu, L., Henault, M., Thomas, E., Yeola, S., Lao, J., McPate, M., Verkuyl, J.M., et al. (2015). Englerin A agonizes the TRPC4/C5 cation channels to inhibit tumor cell line proliferation. PLoS One *10*, e0127498.

Chinnery, P., and Hudson, G. (2013). Mitochondrial genetics. Br. Med. Bull. *106*, 135–159.

Corazao-Rozas, P., Guerreschi, P., Jendoubi, M., Andre, F., Jonneaux, A., Scalbert, C., Garcon, G., Malet-Marino, M., Balayssac, S., Rocchi, S., et al.

(2013). Mitochondrial oxidative stress is the Achille's heel of melanoma cells resistant to Braf-mutant inhibitor. Oncotarget *4*, 1986–1998.

Das Thakur, M., Salangsang, F., Landman, A.S., Sellers, W.R., Pryer, N.K., Levesque, M.P., Dummer, R., McMahon, M., and Stuart, D.D. (2013). Modelling vemurafenib resistance in melanoma reveals a strategy to forestall drug resistance. Nature *494*, 251–255.

Davies, H., Bignell, G.R., Cox, C., Stephens, P., Edkins, S., Clegg, S., Teague, J., Woffendin, H., Garnett, M.J., Bottomley, W., et al. (2002). Mutations of the BRAF gene in human cancer. Nature *417*, 949–954.

Dias, D., Urban, S., and Roessner, U. (2012). A historic overview of natural products in drug discovery. Metabolites *2*, 303–336.

Druckova, A., Mernaugh, R., Ham, A.-J., and Marnett, L. (2007). Identification of the protein targets of the reactive metabolite of teucrin A in vivo in the rat. Chem. Res. Toxicol. *20*, 1393–1408.

Druckovia, A., and Marnett, L. (2006). Characterization of the amino acid adducts of the enedial derivative of teucrin A. Chem. Res. Toxicol. *19*, 1330–1340.

Du, J., Miller, A.J., Widlund, H.R., Horstmann, M.A., Ramaswamy, S., Fisher, D.E., et al. (2003). MLANA/MART1 and SILV/PMEL17/GP100 are transcriptionally regulated by MITF in melanocytes and melanoma. Am. J. Pathol. *163*, 333–343.

Ehrhardt, M., Gerber, A., Hannemann, F., and Bernhardt, R. (2016). Expression of human CYP27A1 in B. megaterium for the efficient hydroxylation of cholesterol, vitamin D3 and 7-dehydrocholesterol. J. Biotechnol. *218*, 34–40.

Garraway, L., Widlund, H.R., Rubin, M.A., Getz, G., Berger, A.J., Ramaswamy, S., Beroukhim, R., Milner, D.A., Granter, S.R., Du, J., et al. (2005). Integrative genomic analyses identify MITF as a lineage survival oncogene amplified in malignant melanoma. Nature *436*, 117–122.

Gupta, R., Patrick, K., and Bell, N. (2007). Mutational analysis of CYP27A1: assessment of 27-hydoxylation of cholesterol and 25-hydroxylation of vitamin D. Metabolism *56*, 1248–1255.

Hanahan, D., and Weinberg, R. (2011). Hallmarks of cancer: the next generation. Cell *144*, 646–674.

Haq, R., Shoag, J., Andreu-Perez, P., Yokoyama, S., Edelman, H., Rowe, G.C., Frederick, D.T., Hurley, A.D., Nellore, A., Kung, A.L., et al. (2013). Oncogenic BRAF regulates oxidative metabolism via PGC1alpha and MITF. Cancer Cell *23*, 302–315.

Harvey, A. (2008). Natural products in drug discovery. Drug Discov. Today *13*, 894–901.

Harvey, A., Edrada-Ebel, R., and Quinn, R. (2015). The re-emergence of natural products for drug discovery in the genomics era. Nat. Rev. Drug Discov. *14*, 111–129.

Hodis, E., Watson, I.R., Kryukov, G.V., Arold, S.T., Imielinski, M., Theurillat, J.-P., Nickerson, E., Auclair, D., Li, L., Place, C., et al. (2012). A landscape of driver mutations in melanoma. Cell *150*, 251–263.

Hoek, K., Schlegel, N.C., Eichhoff, O.M., Widmer, D.S., Praetorius, C., Einarsson, S.O., Valgeirsdottir, S., Bergsteinsdottir, K., Schepsky, A., Dummer, R., et al. (2008). Novel MITF targets identified using a two-step DNA microarray strategy. Pigment Cell Melanoma Res *21*, 665–676.

Hou, L., Panthier, J., and Arnheiter, H. (2000). Signaling and transcriptional regulation in the neural crest-derived melanocyte lineage: interactions between KIT and MITF. Development *127*, 5379–5389.

Kauffmann, A., Gentleman, R., and Huber, W. (2009). arrayQualityMetrics–a bioconductor package for quality assessment of microarray data. Bioinformatics *25*, 415–416.

Keith, C., Borisy, A., and Stockwell, B. (2005). Multicomponent therapeutics for networked systems. Nat. Rev. Drug Discov. *4*, 71–78.

Khuong-Huu, Q., Chiaroni, A., Riche, C., Nguyen-Ngoc, H., Nguyen-Viet, K., Khuong-Huu, F., et al. (2000). New rearranged limonoids from Harrisonia perforata. J. Nat. Prod. *63*, 1015–1018.

Kornienko, A., and La Clair, J. (2017). Covalent modification of biological targets with natural products through Paal-Knorr pyrrole formation. Nat. Prod. Rep. *34*, 1051–1060.

Lai, K., Selinger, D.W., Solomon, J.M., Wu, Hua, Schmitt, E., Serluca, F.C., Curtis, D., and Benson, J.D. (2013). Integrated compound profiling screens identify the mitochondrial electron transport chain as the molecular target of the natural products manassantin, sesquicillin, and arctigenin. ACS Chem. Bio. *8*, 257–267.

Langmead, B., and Salzberg, S. (2012). Fast gapped-read alignment with Bowtie2. Nat. Methods *9*, 357–359.

Law, C., Chen, Y., Shi, W., and Smyth, G. (2014). voom: precision weights unlock linear model analysis tools for RNA-seq read counts. Genome Biol. *15*, R29.

Lekehal, M., Pessayre, D., Lereau, J.M., Moulis, C., Fouraste, I., and Fau, D. (1996). Hepatotoxicity of the herbal medicine germander: metabolic activation of its furano diterpenoids by cytochrome P450 3A depletes cytoskeleton-associated protein thiols and forms plasma membrane blebs in rat hepatocytes. Hepatology *24*, 212–218.

Lin, W., Baker, A.C., Beroukhim, R., Winckler, W., Feng, W., Marmion, J.M., Laine, E., Greulich, H., Tseng, H., Gates, C., et al. (2008). Modeling genomic diversity and tumor dependency in malignant melanoma. Cancer Res. *68*, 664–673.

Lin, D., Li, C., Peng, Y., Gao, H., and Zheng, J. (2014). Cytochrome P450-mediated metabolic activation of diosbulbin B. Drug Metab. Dispos *42*, 1727–1736.

Lin, D., Wang, K., Guo, X., Gao, H., Peng, Y., and Zheng, J. (2016). Lysine- and cysteine-based protein adductions derived from toxic metabolites of 8-epi-diosbulbin E acetate. Toxicol. Lett *264*, 20–28.

MacKinnon, S., Durst, T., Arnason, J.T., Angerhofer, C., Pezzuto, J., Sanchez-Vindas, P.E., Poveda, L.J., and Gbeassor, M. (1997). Antimalarial activity of tropical Meliaceae extracts and gedunin derivatives. J. Nat. Prod. *60*, 336–341.

Manners, G. (2007). Citrus limonoids: analysis, bioactivity, and biomedical prospects. J. Agric. Food Chem. *55*, 8285–8294.

Marroquin, L., Hynes, J., Dykens, J.A., Jamieson, J.D., and Will, Y. (2007). Circumventing the Crabtree effect: replacing media glucose with galactose increases susceptibility of HepG2 cells to motochondrial toxicants. Toxicol. Sci. *97*, 539–547.

Mast, N., Lin, J., and Pikuleva, I. (2015). Marketed drugs can inhibit cytochrome p450 27A1, a potential new target for breast cancer adjuvant therapy. Mol. Pharmacol. *88*, 428–436.

Melnick, J., Janes, J., Kim, S., Chang, J.Y., Sipes, D.G., Gunderson, D., Jarnes, L., Matzen, J.T., Garcia, M.E., Hood, T.L., et al. (2006). An efficient rapid system for profiling the cellular activities of molecular libraries. Proc. Natl. Acad. Sci. USA *103*, 3153–3158.

Miller, D., Adam, M.P., Aradhya, S., Biesecker, L.G., Brothman, A.R., Carter, N.P., Church, D.M., Crolla, J.A., Eichler, E.E., Epstein, C.J., et al. (2010). Consensus statement: chromosomal microarray is a first-tier clinical diagnostic test for individuals with developmental disabilities or congenital anomalies. Am. J. Hum. Genet. *86*, 749–764.

Mishra, P., and Chan, D. (2014). Mitochondrial dynamics and inheritance during cell division, development and disease. Nat. Rev. Mol. Cell. Biol. *15*, 634–646.

Moro, S., Chipman, J.K., Antczak, P., Turan, N., Dekant, W., Falciani, F., and Mally, A. (2012). Identification and pathway mapping of furan target proteins reveal mitochondrial energy production and redox regulation as critical targets of furan toxicity. Toxicol. Sci. *126*, 336–352.

Newman, D., and Cragg, G. (2016). Natural products as sources of new drugs from 1981 to 2014. J. Nat. Prod. *79*, 629–661.

Pikuleva, I., Cao, C., and Waterman, M. (1999). An additional electrostatic interaction between adrenodoxin and p450c27 (CYP27A1) results in tighter binding than between adrenodoxin and p450scc (CYP11A1). J. Biol. Chem. *274*, 2045–2052.

Corcoran, R., Dias-Santagata, D., Bergethon, K., Iafrate, A.J., Settleman, J., and Engelman, J.A. (2010). BRAF gene amplification can promote acquired resistance to MEK inhibitors in cancer cells harboring the BRAF V600E mutation. Sci. Signal. *3*, ra84.

da Richa, A., Lopes, R., and Schwartsmann, G. (2001). Natural products in anticancer therapy. Curr. Opin. Pharmacol. *1*, 364–369.

Ritchie, M.E., Phipson, B., Wu, D., Hu, Y., Law, C.W., Shi, W., and Smyth, G.K. (2015). Limma powers differential expression analyses for RNA-sequencing and microarray studies. Nucleic Acids Res. *43*, e47.

Roesch, A., Vultur, A., Bogeski, I., Wang, H., Zimmermann, K.M., Speicher, D., Korbel, C., Laschke, M.W., Gimotty, P.A., Philipp, S.E., et al. (2013). Overcoming intrinsic multidrug resistance in melanoma by blocking the mitochondrial respiratory chain of slow-cycling JARID1B(high) cells. Cancer Cell *23*, 811–825.

Roy, A., and Saraf, S. (2006). Limonoids: overview of significant bioactive triterpenes distributed in plant kingdom. Biol. Pharm. Bull. *29*, 191–201.

Salma, N., Song, J.S., Kawakami, A., Devi, S.P., Khaled, M., Cacicedo, J.M., and Fisher, D.E. (2017). Tfe3 and Tfeb transcriptionally regulate Ppargamma2 expression in adipocytes and mediate adiponectin and glucose levels in mice. Mol. Cell. Biol. *37*, e00608–e00616.

Schneider, H., Berthold, J., Bauer, M.F., Dietmeier, K., Guiard, B., Brunner, M., and Neupert, W. (1994). Mitochondrial Hsp70/MIM44 complex facilitates protein import. Nature *371*, 768–774.

Schneider, C., Rasband, W., and Eliceiri, K. (2012). NIH Image to ImageJ: 25 years of image analysis. Nat. Methods *9*, 671–675.

Schockel, L., Glasauer, A., Basit, F., Bitschar, K., Truong, H., Erdmann, G., Algire, C., Hagebarth, A., Willems, P.H.G.M., Kopitz, C., et al. (2015). Targeting mitochondrial complex I using BAY 87-2243 reduces melanoma tumor growth. Cancer Metab. *3*, 11.

Schuierer, S., and Roma, G. (2016). The exon quantification pipeline (EQP): a comprehensive approach to the quantification of gene, exon and junction expression from RNA-seq data. Nucleic Acids Res. *44*, e132.

Shen, B. (2015). A new golden age of natural product drug discovery. Cell *163*, 1297–1300.

Shi, H., Hugo, W., Kong, X., Hong, A., Koya, R.C., Moriceau, G., Chodon, T., Guo, R., Johnson, D.B., Dahlman, K.B., et al. (2014). Acquired resistance and clonal evolution in melanoma during BRAF inhibitor therapy. Cancer Discov. *4*, 80–93.

Shi, H., Moriceau, G., Kong, X., Lee, M.-K., Lee, H., Koya, R.C., Ng, C., Chodon, T., Scolyer, R.A., Dahlman, K.B., et al. (2012). Melanoma whole-exome sequencing identifies (V600E)B-RAF amplification-mediated acquired B-RAF inhibitor resistance. Nat. Commun. *3*, 724.

Shoemaker, R. (2006). The NCI60 human tumor cell line anticancer drug screen. Nat. Rev. Cancer *6*, 813–823.

Shtivelman, E., Davies, M.A., Hwu, P., Yang, J., Lotem, M., Oren, M., Flaherty, K.T., and Fisher, D.E. (2014). Pathways and therapeutic targets in melanoma. Oncotarget *5*, 1701–1752.

Sigoillot, F., Lyman, S., Huckins, J.F., Adamson, B., Chung, E., Quattrochi, B., and King, R.W. (2012). A bioinformatics method identifies prominent off-targeted transcripts in RNAi screens. Nat. Methods *9*, 363–366.

Spek, A. (2003). Single-crystal structure validation with the program PLATON. J. Appl. Cryst. *36*, 7–13.

Spradlin, J., Hu, X., Ward, C.C., Brittain, S.M., Jones, M.D., Ou, L., To, M., Proudfoot, A., Ornelas, E., Woldegiorgis, M., et al. (2019). Harnessing the anti-cancer natural product nimbolide for targeted protein degradation. Nat. Chem. Bio. *15*, 747–755.

Tieu, E., Li, W., Chen, J., Baldisseri, D.M., Slominski, A.T., and Tuckey, R.C. (2012). Metabolism of cholesterol, vitamin D3, and 20-hydroxyvitamin D3 incorporated into phospholipid vesicles by human CYP27A1. J. Steroid Biochem. Mol. Biol. *129*, 163–171.

Wagle, N., Van Allen, E.M., Treacy, D.J., Frederick, D.T., Cooper, Z.A., Taylor-Wheeler, A., Rosenberg, M., Goetz, E.M., Sullivan, R.J., Farlow, D.N., et al. (2014). MAP kinase pathway alterations in BRAF-mutant melanoma patients with acquired resistance to combined RAF/MEK inhibition. Cancer Discov. *4*, 61–68.

Wang, C., Weerapana, E., Blewett, M.M., and Cravatt, B.F. (2014). A chemoproteomic platform to quantitatively map targets of lipid-derived electrophiles. Nat. Methods *11*, 79–85.

Warburg, O. (1956). On respiratory impairment in cancer cells. Science *124*, 269–270.

Webster, D., Barajas, B., Bussat, R.T., Yan, K.J., Neela, P.H., Flockhart, R.J., Kovalski, J., Zehnder, A., and Khavari, P.A. (2014). Enhancer-targeted genome editing selectively blocks innate resistance to oncokinase inhibition. Genome Res. *24*, 751–760.

Weerapana, E., Wang, C., Simon, G.M., Richter, F., Khare, S., Dillon, M.B.D., Bachovchin, D.A., Mowen, K., Baker, D., and Cravatt, B.F. (2010). Quantitative reactivity profiling predicts functional cysteines in proteomes. Nature *468*, 790–795.

Wen, S., Zhang, F., and Feng, S. (2013). Decreased copy number of mitochondrial DNA: a potential diagnostic criterion for gastric cancer. Oncol. Lett. *6*, 1098–1102.

Xu, T., Park, S.K., Venable, J.D., Wohlschlegel, J.A., Diedrich, J.K., Cociorva, D., Lu, B., Liao, L., Hewel, J., Han, X., et al. (2015). ProLuCID: an improved SEQUEST-like algorithm with enhanced sensitivity and specificity. J. Proteomics *129*, 16–24.

Yan, X.-H., Di, Y.-T., Fang, X., Yang, S.-Y., He, H.-P., Li, S.-L., Lu, Y., and Hao, X.-J. (2011). Chemical constituents from fruits of *Harrisonia perforata*. Phytochemistry *72*, 508–513.

Yan, X.-H., Yi, P., Cao, P., Yang, S.-Y., Fang, X., Zhang, Y., Wu, B., Leng, Y., Di, Y.-T., Lv, Y., et al. (2016). 16-nor limonoids from *Harrisonia perforata* as promising selective 11B-HSD1 inhibitors. Sci. Rep. *6*, 36927.

Zhang, G., Frederick, D.T., Wu, L., Wei, Z., Krepler, C., Srinivasan, S., Chae, Y.C., Xu, X., Choi, H., Dimwamwa, E., et al. (2016). Targeting mitochondrial biogenesis to overcome drug resistance to MAPK inhibitors. J. Clin. Invest. *126*, 1834–1856.

Zhang, W., Zhang, Z., Tang, J.-C., Che, J.-T., Zhang, H.-Y., Chen, J.-H., and Yang, Z. (2020). Total synthesis of (+)-haperforin G. J. Am. Chem. Soc. *142*, 19487–19492.

Please cite this article in press as: Cho et al., CYP27A1-dependent anti-melanoma activity of limonoid natural products targets mitochondrial metabolism, Cell Chemical Biology (2021), https://doi.org/10.1016/j.chembiol.2021.03.004

STAR★METHODS

KEY RESOURCES TABLE

REAGENT or RESOURCE	SOURCE	IDENTIFIER
Antibodies		
PhosphoPlus® p38 MAPK (Thr180/Tyr182) Antibody Duet	Cell Signaling Technology	Cat#8203
PhosphoPlus® MEK1/2 (Ser217/Ser221) Antibody Duet	Cell Signaling Technology	Cat#8211
PhosphoPlus® p44/42 MAPK (Erk1/2) (Thr202/Tyr204) Antibody Duet	Cell Signaling Technology	Cat#8201
Anti-alpha Tubulin antibody [DM1A]	Abcam	ab7291
Phospho-B-Raf (Ser445) Antibody	Cell Signaling Technology	Cat#2696
Microphthalmia (Transcription Factor) (MiTF) Ab-1 (C5)	Thermo Scientific	MS-771-P1
MitoBiogenesis™ Western Blot Cocktail	Abcam	ab123545
Total OXPHOS Human WB Antibody Cocktail	Abcam	ab110411
TFAM (D5C8) Rabbit mAb	Cell signaling	Cat#8076
Recombinant Anti-Alas1 antibody [EPR10247]	Abcam	ab154860
Anti-CYP27A1 antibody	Sigma-Aldrich	ab82926
Monoclonal Anti-β-Actin antibody produced in mouse	Sigma-Aldrich	A5441
Bacterial and virus strains		
Bacillus megaterium	Ehrhardt et al. (2016)	N/A
Chemicals, peptides, and recombinant proteins		
MG-132	Selleck Chemicals	S2619-5MG (CAS 1211877-36-9)
MitoTracker™ Green FM	Invitrogen™	M7514
Vybrant® DyeCycle™ Green Stain	Invitrogen™	V35004
FxCycle™ PI/RNAse Staining Solution	Invitrogen™	F10797
Glucose Solution	Invitrogen	A2494001
20% Galactose Solution	Teknova	G0505
Fetal Bovine Serum	Gibco™	Cat#10082147
Penicillin-Streptomycin (5,000 U/mL)	Gibco™	Cat#15070063
L-Glutamine (200 mM)	Gibco™	Cat#25030149 (CAS 56-85-9)
RIPA lysis and extraction buffer	Invitrogen	Cat#89900
DMSO (Hybri-Max™, sterile-filtered, BioReagent, suitable for hybridoma, ≥99.7%)	Sigma-Aldrich	D2650-5X5ML (CAS 67-68-5)
Rotenone	Enzo lifesciences	ALX-350-360-G001 (CAS 83-79-4)
Antimycin A	Alfa aeser	J63522 (CAS 1397-94-0)
Tetramethylrhodamine, Methyl Ester, Perchlorate (TMRM)	Invitrogen™	T668 (CAS 115532-50-8)
Hoechst 33342 Solution	Thermo Scientific	Cat#62249 (CAS 875756-97-1)
Iodoacetamide, 98%	ACROS Organics	Cat#31985062
Urea	Fisher Chemical	U15-500 (CAS 57-13-6)
ProteaseMAX Surfactant, lyopholized	Promega	REF#V2072
Ammonium Bicarbonate	Fisher Chemical	A643-500 (CAS 1066-33-7)
TCEP 99%	Strem Chemicals	Cat#15-7400 (CAS 51805-45-9)

(*Continued on next page*)

Please cite this article in press as: Cho et al., CYP27A1-dependent anti-melanoma activity of limonoid natural products targets mitochondrial metabolism, Cell Chemical Biology (2021), https://doi.org/10.1016/j.chembiol.2021.03.004

Continued

REAGENT or RESOURCE	SOURCE	IDENTIFIER
Formic Acid, 99.0+%, Optima LC/MS Grade	Fisher Chemical	A117-50 (CAS 64-18-6)
Sequencing Grade Modified Trypsin, Porcine	Promega	V511A
Laemmli SDS sample buffer, reducing (4x)	Alfa Aesar	J60015
Tris(benzyltriaxole methylamine) (TBTA)	Sigma-Aldrich	Cat#678937 (CAS 510758-28-8)
Biotin-TEV-azide	Weerapana et al., 2010	N/A
Copper (II) sulfate	Sigma-Aldrich	Cat#451657
AcTEV Protease	Invitrogen™	Cat#12575-015
N-Hex-5-ynyl-2-iodo-acetamide (IA-alkyne)	Chess Gmbh	Cat#3187
Pierce protease inhibitor mini tablets, EDTA-free	Thermo Scientific	A32955
High Capacity Streptavidin Agarose Resin	Thermo Scientific	Cat#20357
Streptavidin Agarose Resin	Thermo Scientific	Cat#20349
MKT-077	Sigma-Aldrich	M5449-5MG (CAS 147366-41-4)
Fadrozole	Novartis compound library	N/A (CAS 102676-31-3)
Dabrafenib	Novartis compound library	N/A (CAS 1195765-45-7)
Trametinib	Novartis compound library	N/A (CAS 871700-17-3)
CCCP (Carbonyl cyanide m-chlorophenyl hydrazone)	Novartis compound library	N/A (CAS 555-60-2)
Critical commercial assays		
CellTiter-Glo® Luminescent Cell Viability Assay	Promega	G7571
CellTox™ Green Cytotoxicity Assay	Promega	G8741
RealTime ready DNA Probes Master, 5 x 1 ml	Roche	Cat#5502381001
Mitochondria Isolation Kit for Cultured Cells	Thermo Scientific	89874
MitoTracker™ Red CMXRos	Invitrogen™	M7512
MITF TaqMan™ Gene Expression Assay	Applied Biosystems™	4453320 (Hs01117294_m1)
Click-iT® Plus EdU Alexa Fluor® 488 Flow Cytometry Assay Kit	Invitrogen™	C10632
Mitochondrial Membrane Potential Indicator	Codex BioSolutions	CB80600010
Agilent Seahorse XF Cell Mito Stress Test Kits	Agilent Technologies	Cat#103015-100
Deposited data		
Small molecule x-ray structure of harrpernoid D	Cambridge Crystallographic Data Center (CCDC); ccdc.cam.ac.uk	Cat#2061432
Experimental models: Cell lines		
Cell lines used in this study	Novartis cell line encyclopedia collection	N/A (Barretina et al., 2012); Data S1
Oligonucleotides		
See Data S1 Oligonucleotides Reagents tab		
Recombinant DNA		
pCDH-CMV-MCS-EF1α-Puro lentiviral vector	System Biosciences	CD510B-1
pTurboGFP-mito vector	Clontech	632432
Sigma CRISPR dCas9-p300 Activator Expression Plasmid	Sigma-Aldrich	DCAS9P300-1EA
Software and algorithms		
ImageJ	(Schneider, et al., 2012)	https://imagej.nih.gov/ij/

(*Continued on next page*)

Please cite this article in press as: Cho et al., CYP27A1-dependent anti-melanoma activity of limonoid natural products targets mitochondrial metabolism, Cell Chemical Biology (2021), https://doi.org/10.1016/j.chembiol.2021.03.004

Continued

REAGENT or RESOURCE	SOURCE	IDENTIFIER
IP2 proteomics pipeline 5.0.1	Integrated Proteomics Applications	N/A
Pipeline pilot	Biovia - Dassault Systèmes®	N/A
PLATON	(Spek, 2003)	https://www.platonsoft.nl/platon/

RESOURCE AVAILABILITY

Lead contact

Further information and request for resources and reagents will be fulfilled by the lead contact, William Forrester, william.forrester@novartis.com.

Materials availability

Plasmids and compounds generated in this study will be made available upon reasonable request. Material supply of haperforin G, haperforin C2, and harrpernoid D are limited and subject to handling under Nagoya protocol.

Data and code availability

The RNA-Seq data are available in the Sequence Read Archive (http://www.ncbi.nlm.nih.gov) with accession number SRP108654. Data generated in this study will be made available upon reasonable request. No code was developed for this study.

EXPERIMENTAL MODEL AND SUBJECT DETAILS

Cell lines used in this study are part of the Novartis Cancer Cell Line Encyclopedia collection (CCLE). Detailed information about these cell lines (including gender, primary site (tumor type), source) are described in (Barretina et al., 2012) and are also included in Data S1.

METHOD DETAILS

Cell line profiling

Cell line profiling experiment was performed as described (Carson et al., 2015). All assays were automated and performed with an ultra-high throughput screening system built by the Genomics Institute of the Novartis Research Foundation (Melnick et al., 2006) (http://www.gnfsystems.com). Briefly, 498 cell lines across 25 tissue lineages (Data S1) were plated into 1,536-micro plates (Greiner) at a density of 250 cells per well with a final volume of 5μL. 12 to 24 hours after plating, 15 nL of each compound dilution series was transferred to the cells using an Echo acoustic liquid dispenser (Labcyte) to yield final compound concentration ranges of 30 μM to 0.3μM (11 point dose response) in 3.16-fold dilutions. Cell viability was determined by CellTiter-Glo (Promega) 72 hours after compound treatment and data was captured using ViewLux plate reader (Perkin Elmer) according to the manufacturer's instructions. Absolute maximum cytotoxicity for each cell line was benchmarked against the impact on viability by exposure to 10μM of MG132 (proteasome inhibitor that shows pan-toxicity).

Cell lines and Cell culture

Melanoma cell lines were obtained from the Novartis cell line encyclopedia collection (Barretina et al., 2012) and were cultured in RPMI 1640 medium containing 10% Fetal Bovine Serum (FBS), 1% penicillin/streptomycin (P/S), and 2mM Glutamine.

Cell line manipulation

CYP27A1$^{-/-}$ cell line clones were generated using CRISPR-Cas9 (pU6g-cas9-puromycin; gift from Dr. Yi Yang at Novartis) mediated knockout followed by single-cell sorting. Loss of CYP27A1 protein expression and homogenous biallelic knockout of *CYP27A1* in each cell clones was confirmed by Western blot analysis and sequencing. For *CYP27A1*-overexpressing cell lines, *CYP27A1* cDNA was cloned into pCDH lentiviral vector (System Biosciences), cells then were transduced with packaged lentivirus and selected for stable expression of *CYP27A1* using antibiotics treatment (1000μg/mL neomycin or 2μg/mL puromycin as indicated).

Generation of BRAFi/MAPKi resistant cell lines

Resistant cell lines (MEL-HO and UACC257) were generated as described previously (Corcoran et al., 2010). Briefly, dabrafenib or combination of dabrafenib and trametinib was added at a starting concentration of 10 nM (dabrafenib) or 0.316 nM (trametinib), and cells were maintained in fresh drug-containing medium changed every 72 hours. Cells were passaged when they reached ~70% confluence. After every two or three passages at a given concentration of drug, the concentration of drug was increased in half-log intervals until a final concentration was achieved.

Please cite this article in press as: Cho et al., CYP27A1-dependent anti-melanoma activity of limonoid natural products targets mitochondrial metabolism, Cell Chemical Biology (2021), https://doi.org/10.1016/j.chembiol.2021.03.004

Cell viability/cytotoxicity assay

Cells were plated into each well of Greiner 384-well plates at a density of 1,500 cells/well. Cells were incubated with increasing concentration of compounds (0.1% vol/vol DMSO) for 72 to 96 hours and cell viability/cytotoxicity was measured by EnVison plate reader (Perkin Elmer) with CellTiter-Glo (Promega) or CellTox Green (Promega) according to the manufacturer's protocol.

Glucose-Galactose assay

Mitochondrial toxicity by compound was assessed by Glucose-Galactose assay as described previously (Lai et al., 2013).

Cell cycle analysis/cell proliferation assay

For S phase analysis, cells were stained using Click-iT® EdU Alexa Fluor® 488 Flow Cytometry Assay Kit (Thermo Fisher Scientific) according to the manufacturer's instructions. To distinguish cells in G0/G1 phase versus S phase, or G2, cells were stained using FxCycle™ PI/RNase Staining Solution (Thermo Fisher Scientific) according to the manufacture's protocol. Cells were analyzed using BD FACSCANTO II (BD Biosciences) and FlowJo software.

ChIP-qPCR

ChIP was performed as described previously (Salma et al., 2017). Briefly, protein:chromatin-crosslinked complexes were immunoprecipitated with either MITF-specific antibody (Cell Signaling) or isotype control antibody. qRT-PCR was performed on samples to amplify a fragment occupied by MITF using primers spanning promoter region of *CYP27A1, TYR*, or *RPL11* gene body. Primers used were: 5'- GGAAGGCCATTGGGAGAAG-3' and 5'-GATTCTTTCGAAATCGGGAAGC-3' for *CYP27A1* promoter, 5'-GTGGGATAC GAGCCAATTCGAAAG-3' and 5-TCCCACCTCCAGCATCAAACACTT-3' for *TYR*, and 5-ACACAGATCATGGGTCTTGCTCCA-3' and 5-AGCACCTGTCCCAGGAATAACCAA-3' for *RPL11* gene body.

Western blot analysis

Whole cell lysates were isolated with RIPA Lysis and Extraction buffer (Thermo Fisher Scientific) supplemented with Halt™ protease and phosphatase inhibitor cocktail (Thermo Fisher Scientific) according to the manufacturer's protocol. All antibodies used were from Cell Signaling except for: CYP27A1 (Abcam), Mitobiogenesis cocktail (Abcam), Alas1 (abcam), MITF (Thermo Fisher Scientific)

Subcellular fractionation

Subcellular fractionation and mitochondria isolation was performed by using differential centrifugation with Mitochondria Isolation Kit (Thermo Scientific) according to the manufacturer's protocol.

High-content imaging

High-content staining for mitochondria, TFAM, SDHA was performed using an IN Cell Analyzer 6000 Cell Imaging System (GE Healthcare Life Sciences). Antibodies used were: MitoTracker® Red CMXRos (Thermo Fisher Scientific), TFAM (D5C8) (Cell Signaling), SDHA (D6J9M) (Cell Signaling)

mtDNA copy number analysis

Total genomic DNA was isolated using QIAamp DNA Kit (QIAGEN) and a quantitative PCR method was used to determine the mtDNA copy number as described (Wen, et al., 2013). The primers of β-actin (product length, 138 bp) were forward, 5′-CGGG AAATCGTGCGTGACAT-3′ and reverse, 5′-GAA GGAAGGCTGGAAGAGTG-3′. The primers of mtDNA (product length, 487 bp) were forward, 5′-TACTCACCAGACGCCTCAACCG-3′ and reverse, 5′-TTA TCGGAATGGGAGGTGATTC-3′.

Quantitation of mitochondrial membrane potential

Mitochondrial membrane potential was measured using mitochondrial membrane potential indicator (MMPI, Codex) according to the manufacturer's instructions.

Metabolic assays

Oxygen consumption rate (OCR) was measured with the optical fluorescent oxygen/hydrogen sensor XFe96 Seahorse analyzer according the manufacturer's protocol. During the continuous OCR measure, the following compounds were sequentially administered: oligomycin 1mM, FCCP 2mM, and rotenone/antimycin A 1mM. The data was normalized to total cell number as measured using the CellTag700 stain and Odyssey imaging system (Li-COR, Lincoln, NE).

Genome-wide RNAi screening

60nL of 2uM siRNAs were stamped using an Echo acoustic liquid dispenser (Labcyte) on each well of 1,536-micro plates (Greiner) for final concentration of 20nM. Cells were then reverse-transfected using Dharmafect 4 (Dharmacon) according to the manufacturer's protocol. 24 hours after transfection, cells were incubated for 96 hours with DMSO (vehicle), IC_{30} of harrpernoid D, or dabrafenib until lysed with CellTiter-Glo (Promega) for viability assay. Luminescence signal was measured with ViewLux microplate reader (Perkin

Please cite this article in press as: Cho et al., CYP27A1-dependent anti-melanoma activity of limonoid natural products targets mitochondrial metabolism, Cell Chemical Biology (2021), https://doi.org/10.1016/j.chembiol.2021.03.004

Elmer) according to the manufacturer's instructions. Screen data were processed using RSA (redundant siRNA activity) analysis and GESS (genome-wide enrichment of seed sequence matches) off-target analysis as described previously (Sigoillot et al., 2012; Birmingham et al., 2009).

RNA-sequencing (RNA-seq)

Three biological replicates of MEL-HO wild-type and MEL-HO *cyp27a1*$^{-/-}$ were treated with DMSO, IC_{20}, and IC_{70} of harrpernoid D (0.1% DMSO vol/vol) for 24 hours, 48 hours, and 72 hours. Total RNA was isolated according to the manufacturer's protocol with an RNeasy kit with on-column DNA digestion (Qiagen). RNA concentration and integrity was measured by fragment analyzer with Standard Sensitivity RNA kit according to the manufacturer's protocol (Advanced Analytical Technologies). RNA-seq libraries were prepared using the TruSeq Stranded mRNA Sample Preparation kit (Illumina) and sequenced in strand specific paired-end mode, 2x76bp, using the HiSeq2500 platform. Alignment against Human Ensembl genome reference GRCh38 (release 78) utilized the exon quantification pipeline (EQP) (Schuierer and Roma, 2016) with the Bowtie2 (Langmead and Salzberg, 2012) alignment module for exon- and gene-level quantitation. Alignment quality was assessed using Picard (http://broadinstitute.github.io/picard/) and ArrayQualityMetrics (Kauffmann, et al., 2009), passing internal criteria. Differential expression comparisons were calculated using limma linear modeling (Ritchie et al., 2015) with voom precision weighting (Law, et al., 2014).

Isolation of harrpernoid D

30 kg leaves of *Harrisona perforate* were milled and extracted with ethyl acetate. The resulting extract was purified using a Daisogel SP 200-15-C8 column using water and methanol as solvents (gradient 30% to 100% methanol). Fractions containing the target molecule were further purified using a Sunfire RP18 column followed by final purification using a Synergi Polar-RP column (0.1% formic acid / acetonitrile containing 0.1% formic acid as solvents). 115 mg pure (>95%) harrpernoid D could be isolated. 1H NMR: (d_6-DMSO) δ 7.90 (1H, d, 5.6Hz), 7.73 (1H, br), 7.72 (1H, m), 6.63 (1H, m), 6.14 (1H, d, 5.6Hz), 5.69 (1H, d, 2.1Hz), 5.23 (1H, s), 4.19 (1H, m), 3.89 (1H, br), 2.68 (1H, dd, 13.5 & 6.1Hz), 1.95 (2H, m), 1.73 (2H, m), 1.64 (1H, m), 1.48 (3H, s), 1.34 (3H, s), 1.34 (1H, m), 1.11 (3H, s), 0.81 (3H, s), The structure was confirmed by x-ray analysis. The measured crystal is a di hydrate. The furanyl ring C27 to C31 is disordered and refined on two positions (A/B): ratio 55:45.

Chemical oxidation of harrpernoid D

Harrpernoid D (1.0 mg, 2.3 μmol, 1.0 eq.) was dissolved in 0.3 mL of acetone-d_6 and placed in an NMR tube under nitrogen atmosphere. To this solution was added at once DMDO-d_6 (23 mM in acetone-d_6, 0.10 mL, 1.0 eq.) and the resulting mixture was let it stand at rt. The conversion was monitored by ^{1}H NMR. After 24 h, most of the harrpenoid D was converted to the enedial which was unstable towards purification: ^{1}H NMR: (600 MHz, acetone-d_6) δ 10.77 – 10.72 (m, 1H), 10.65 – 10.63 (m, 1H), 7.81 – 7.77 (m, 1H), 6.64 – 6.55 (m, 1H), 6.06 – 6.03 (m, 1H), 5.66 – 5.63 (m, 1H), 5.28 – 5.25 (m, 1H), 4.30 – 4.24 (m, 1H), 3.81 – 3.76 (m, 1H), 2.76 – 2.70 (m, 1H), 1.99 – 1.96 (m, 1H), 1.97 – 1.92 (m, 1H), 1.91 – 1.85 (m, 1H), 1.85 – 1.77 (m, 2H), 1.57 (s, 3H), 1.50 – 1.44 (m, 1H), 1.43 (s, 3H), 1.21 – 1.17 (m, 3H), 1.01 – 0.98 (m, 3H). HRMS: (ESI-TOF, m/z) calcd. For $C_{25}H_{29}O_8$ $[M+H]^+$ calc.: 457.1857; found: 457.1861.

CYP27A1 biotransformation assay

Human CYP27A1 was expressed in *Bacillus megaterium* as described (Ehrhardt, et al., 2016). 7.5 uL of substrate solution (harrpernoid D (4 mg/mL) with 10 mg/mL cyclodextrin in EtOH) was added to 5 mL of 100 mM pH 7.0 phosphate buffered saline and 2 mL of suspension buffer (100 mM phosphate, 2 g/L xylose, 0.1 g/L δ-aminolevulinic acid hydrochloride adjusted to a pH of 7.5 with NaOH solution). The mixture was incubated at 30°C and 200 rpm. Each reaction was mixed with 5g of lysozyme and sonicated 6 x 30 seconds, with a small tip 2 sec cycle at 85% power. Then the reactions were incubated for 1h at 30°C and 200 rpm before 2 uL of benzonase (Merck) was added. Additional incubation for 1h at 30°C and 200 rpm before the reactions were frozen in dry ice for storage before analysis. Lysate was extracted with acetonitrile, ethyl acetate, or methanol and analyzed by LC/MS.

IsoTOP-ABPP

IsoTOP-ABPP studies were done as previously reported (Spradlin et al., 2019). Cells were lysed by probe sonication in PBS and protein concentrations were measured by BCA assay35. For *in situ* experiments, cells were treated for 90 min with either DMSO vehicle or covalently acting small molecule (from 1,000× DMSO stock) before cell collection and lysis. Proteomes were subsequently labeled with N-5-Hexyn-1-yl-2-iodoacetamide (IA-alkyne) labeling (100 μM) for 1 h at room temperature. CuAAC was used by sequential addition of tris(2-carboxyethyl) phosphine (1 mM, Sigma), tris[(1-benzyl-1H-1,2,3-triazol-4-yl) methyl]amine (34 μM, Sigma), copper(II) sulfate (1 mM, Sigma) and biotin-linker-azide—the linker functionalized with a tobacco etch virus (TEV) protease recognition sequence as well as an isotopically light or heavy valine for treatment of control or treated proteome, respectively. After CuAAC, proteomes were precipitated by centrifugation at 6,500g, washed in ice-cold methanol, combined in a 1:1 control:treated ratio, washed again, then denatured and resolubilized by heating in 1.2% SDS–PBS to 80C for 5 min. Insoluble components were precipitated by centrifugation at 6,500g and soluble proteome was diluted in 5 mL 0.2% SDS–PBS. Labeled proteins were bound to avidin-agarose beads (170 mL resuspended beads per sample, Thermo Pierce) while rotating overnight at 4C. Bead-linked proteins were enriched by washing three times each in PBS and water, then resuspended in 6 M urea and PBS (Sigma), and reduced in TCEP (1 mM, Sigma), alkylated with iodoacetamide (18 mM, Sigma), before being washed and resuspended in 2 M urea and trypsinized overnight with 0.5 μg ml^{-1} sequencing

Please cite this article in press as: Cho et al., CYP27A1-dependent anti-melanoma activity of limonoid natural products targets mitochondrial metabolism, Cell Chemical Biology (2021), https://doi.org/10.1016/j.chembiol.2021.03.004

grade trypsin (Promega). Tryptic peptides were eluted off. Beads were washed three times each in PBS and water, washed in TEV buffer solution (water, TEV buffer, 100 μM dithiothreitol) and resuspended in buffer with Ac-TEV protease and incubated overnight. Peptides were diluted in water and acidified with formic acid (1.2 M, Spectrum) and prepared for analysis.

Mass spectrometry analysis

Total peptides from TEV protease digestion for isoTOP-ABPP were pressure loaded onto 250 mm tubing packed with Aqua C18 reverse phase resin (Phenomenex no. 04A4299), which was previously equilibrated on an Agilent 600 series high-performance liquid chromatograph using the gradient from 100% buffer A to 100% buffer B over 10 min, followed by a 5 min wash with 100% buffer B and a 5 min wash with 100% buffer A. The samples were then attached using a MicroTee PEEK 360 mm fitting (Thermo Fisher Scientific no. p-888) to a 13 cm laser pulled column packed with 10 cm Aqua C18 reverse-phase resin and 3 cm of strong-cation exchange resin for isoTOP-ABPP studies. Samples were analyzed using an Q Exactive Plus mass spectrometer (Thermo Fisher Scientific) using a five-step Multidimensional Protein Identification Technology (MudPIT) program, using 0, 25, 50, 80 and 100% salt bumps of 500 mM aqueous ammonium acetate and using a gradient of 5–55% buffer B in buffer A (buffer A: 95:5 water:acetonitrile, 0.1% formic acid; buffer B 80:20 acetonitrile:water, 0.1% formic acid). Data were collected in data dependent acquisition mode with dynamic exclusion enabled (60 s). One full mass spectrometry (MS^1) scan (400–1,800 mass-to-charge ratio (m/z)) was followed by 15 MS^2 scans of the nth most abundant ions. Heated capillary temperature was set to 200C and the nanospray voltage was set to 2.75 kV, as previously described.

Data were extracted in the form of MS^1 and MS^2 files using Raw Extractor v.1.9.9.2 (Scripps Research Institute) and searched against the Uniprot human database using ProLuCID search methodology in IP2 v.3 (Integrated Proteomics Applications, Inc.) (Xu et al., 2015) Probe-modified cysteine residues were searched with a static modification for carboxyaminomethylation (+57.02146) and up to two differential modifications for methionine oxidation and either the light or heavy TEV tags (+464.28596 or +470.29977, respectively). Peptides were required to be fully tryptic peptides and to contain the TEV modification. ProLUCID data was filtered through DTASelect to achieve a peptide false-positive rate below 5%. Only those probe-modified peptides that were evident across two out of three biological replicates were interpreted for their isotopic light to heavy ratios. Light versus heavy isotopic probe-modified peptide ratios are calculated by taking the mean of the ratios of each replicate paired light vs. heavy precursor abundance for all peptide spectral matches (PSM) associated with a peptide. The paired abundances were also used to calculate a paired sample t-test p-value in an effort to estimate constancy within paired abundances and significance in change between treatment and control. P-values were corrected using the Benjamini/Hochberg method.

QUANTIFICATION AND STATISTICAL ANALYSIS

Cell line growth curve data were graphed using a nonlinear regression fitting model ([inhibitor] vs. response - four parameters) calculated by GraphPad Prism® software, Version 6.07 (GraphPad Software, Inc. [La Jolla, CA, USA]). Error bars indicate mean ± s.d. of (at least) 3 replicates. qRT-PCR/ChIP-qPCR data were graphed using GraphPad Prism® software, Version 6.07 (GraphPad Software, Inc. [La Jolla, CA, USA]) and error bars indicate mean ± s.d. of (at least) 3 replicates. Cell line confluency was measured IncuCyte™ (Essen BioScience) proliferation assay for live-cell analysis software and error bars indicate mean ± s.d. of 3 replicates. Flow cytometry data and cell cycle analysis was performed using the Univariate Models with Watson Pragmatic algorithm in FlowJo® software. Statistical analysis for cell line transcriptome data was performed by Wilcox test using effect size calculated by mean difference between two arrays of cell lines divided by standard deviation. Box-and-whisker plots indicate the values of median, 25th percentiles, and 75th percentiles. siRNA analysis was performed using the redundant siRNA activity (RSA) method for eight individual siRNAs per gene and GESS (genome-wide enrichment of seed sequence matches) off-target analysis. Detailed statistical methods were described previously (Sigoillot et al., 2012; Birmingham et al., 2009). RNA-seq alignment against Human Ensembl genome reference GRCh38 (release 78) utilized the exon quantification pipeline (EQP) (Schuierer and Roma, 2016) with the Bowtie2 (Langmead and Salzberg, 2012) alignment module for exon- and gene-level quantitation. Alignment quality was assessed using Picard (http://broadinstitute.github.io/picard/) and ArrayQualityMetrics (Kauffmann, et al., 2009), passing internal criteria. Differential expression comparisons were calculated using limma linear modeling (Ritchie et al., 2015) with voom precision weighting (Law, et al., 2014). For quantification of Western blots, bands were quantified using Image J and normalized to protein loading controls. Statistical analysis was performed using a Student's unpaired two-tailed t-test. For isoTOP-ABPP data analysis, data were extracted in the form of MS1 and MS2 files using Raw Extractor v.1.9.9.2 (Scripps Research Institute) and searched against the Uniprot human database using ProLuCID search methodology in IP2 v.3 (Integrated Proteomics Applications, Inc.) (Xu et al., 2015). Cysteine residues were searched with a static modification for carboxyaminomethylation (+57.02146) and up to two differential modifications for methionine oxidation and either the light or heavy TEV tags (+464.28596 or +470.29977, respectively). Peptides were required to be fully tryptic peptides and to contain the TEV modification. ProLUCID data were filtered through DTASelect to achieve a peptide false-positive rate below 5%. Only those probe-modified peptides that were evident across two out of three biological replicates were interpreted for their isotopic light to heavy ratios. For those probe-modified peptides that showed ratios greater than two, we only interpreted those targets that were present across all three biological replicates, were statistically significant and showed good quality MS1 peak shapes across all biological replicates. Light versus heavy isotopic probe-modified peptide ratios are calculated by taking the mean of the ratios of each replicate paired light versus heavy precursor abundance for all peptide-spectral matches associated with a peptide. The paired abundances were also used to calculate a paired sample t-test P value in an effort to estimate constancy in paired abundances and significance in change between treatment and control. P values were corrected using the Benjamini–Hochberg method.